Title
MEASUREMENT OF THE SPIN-CORRELATION PARAMETER CNN IN PROTON-PROTON SCATTERING AT 689 MeV

Author
Dost, Helmut Ernst.

Publication Date
1965-02-05

UCRL-11877

University of California

Ernest O. Lawrence Radiation Laboratory

MEASUREMENT OF THE SPIN-CORRELATION PARAMETER C_{NN} IN PROTON-PROTON SCATTERING AT 689 MeV

Berkeley, California

DISCLAIMER

Research and Development

UCRL-11877

UNIVERSITY OF CALIFORNIA

Lawrence Radiation Laboratory
Berkeley, California

AEC Contract No. W-7405-eng-48

MEASUREMENT OF THE SPIN-CORRELATION PARAMETER C_{NN} IN PROTON-PROTON SCATTERING AT 680 MeV

Helmut Ernst Dost

Thesis

February 5, 1965

MEASUREMENT OF THE SPIN-CORRELATION PARAMETER C_{NN}
IN PROTON-PROTON SCATTERING AT 680 MeV

Contents

MEASUREMENT OF THE SPIN-CORRELATION PARAMETER C_{NN} IN PROTON-PROTON SCATTERING AT 680 MeV

Helmut Ernst Dost

Lawrence Radiation Laboratory
University of California
Berkeley, California

February 5, 1965

ABSTRACT

Using a polarized beam and polarized target we have measured the spin-correlation parameter C_{NN} in proton-proton scattering for an incident-proton laboratory-system kinetic energy of 680 MeV. The polarized beam was made by scattering unpolarized protons from the 184-in. cyclotron in an external first target of liquid hydrogen resulting in a polarization of 0.44. To reverse the beam polarization, the incident-proton scattering angle was reversed. The target protons were polarized by a solid-state technique called "dynamic polarization" to 0.40 on the average. The elastic proton-proton interactions involving the polarized protons were kinematically separated from other interactions by counting both protons in coincidence. The angular region covered by the 13 data points extends from 51.2 to 88.7 deg in the center-of-mass system. The results show that C_{NN} rises in this region from about 0.5 to 0.9 with a typical standard deviation of 0.1.

I. INTRODUCTION

One of the principal aims of work in high-energy physics is a coherent description of particle interactions. According to theory, in any of its present-day alternatives, various scattering experiments should be related to one another. Qualitative relations have been shown to be valid, but quantitative relations between different scattering processes are restricted, as yet, to trivial cases.

While high-energy physics deals with a great variety of particles, it seems reasonable to expect that scattering processes involving only pions and nucleons should constitute a separable problem, almost independent of processes involving particles of non-zero strangeness such as K mesons and Λ particles. The validity of this point of view rests in part on the fact that in high-energy collisions K-particle production is materially lower than one would expect from a statistical model, relative to pion production.

Taking the point of view that scattering processes involving pions and nucleons do constitute a separable domain, it seems reasonable to hope that these processes can be quantitatively interrelated. If this is to occur, the theory should be tested for its ability correctly to predict the detailed scattering amplitudes. Conversely, the detailed amplitudes may perhaps be used to suggest the form of terms that a correct theory must include. It is with this general purpose that we seek to make experimental determinations of the scattering amplitudes in complete detail, particularly for systems of pions and nucleons. The experiment described in this paper constitutes one of many experiments that will be required.

In this chapter we remind the reader of the need for nucleon-nucleon elastic-scattering data that will eliminate existing ambiguities in nucleon-nucleon phase shifts. We also relate the various experiments that can be undertaken and the parameters thus measured. Also we try to demonstrate the usefulness of the recently developed polarized proton target as a tool to measure these parameters.

A. Motivation

Moravcsik has reviewed the three general approaches to the nucleon-nucleon interaction: phenomenological, meson theories of the static potential, and dispersion theoretic.[1] In all cases one arrives at a formalism based on model-dependent assumptions and supplied generously with parameters for the sake of flexibility. The examples that readily come to mind are the parameters involved in phenomenological potential models, such as radius of hard core, well depth and radius, wall thickness, etc. Ultimately the theoretical parameters must be evaluated according to experimental results. These are most conveniently expressed in terms of phase shifts. However, unless one discriminates in selecting appropriate experiments, one ends up with data yielding several possible sets of phase shifts, each a candidate that fits the inappropriate experimental data more or less well. It is convenient to discuss the relation between phase shifts and experiment in terms of the scattering matrix of Wolfenstein and Ashkin,[2] or of Stapp in different form.[3] The correct phase shifts at one energy can be obtained from the complete scattering matrix at that energy. An appropriate complete set of experiments yields suitable parameters in terms of which one expresses the scattering matrix.

What constitutes such a complete set of experimental parameters is discussed by Schumacher and Bethe[4] and others. Here we state only that for nucleon-nucleon scattering one must measure eleven carefully chosen parameters at one energy and angle in each of the two isotopic-spin states, to determine the various amplitudes of the scattering matrix unambiguously. If measured at all angles the total number of parameters is reduced from eleven to five in each isotopic-spin state, if one is constructing the scattering matrix at an energy below the inelastic threshold. Unitarity of the scattering matrix then expresses the imaginary parts of scattering-matrix amplitudes at one angle in terms of integrals over all angles of products of the five measured parameters.

To date there is no energy for which a complete set of proton-proton data exists, much less proton-neutron data, since some of the parameters are quite difficult to measure for various reasons mentioned later. (Perhaps unusual circumstances are involved in the case of the sizable set of proton-proton parameters at 310 MeV. It is incomplete because the Berkeley 184-in. cyclotron was modified and came back into operation with more than twice the original energy.) Thus the phase-shift hunter must use data at several different energies in conjunction with sufficient model-dependent assumptions about the behavior of the phase shifts in the intermediate energy regions to yield an "unambiguous" set of phase shifts. With these he then hopes to test the model. The situation seems to represent a mandate to the experimenter to develop new techniques to measure those less accessible parameters.

It is a step in the right direction to simply accumulate experimenal data even if they are uncorrelated in energy. Any additional data reduces the degree to which one needs to bridge the energy gaps with poorly tested assumptions. This represents in part the motivation for the present experiment. For quite clearly the beam energy was not picked to complement existing data but rather because it was easily available. Since the experimental accuracy was limited only by counting statistics, it was thought desirable to work with the highest flux possible. Further motivation was simply to test the ease with which the recently developed polarized-proton target measures one of the more difficult polarization parameters.

B. Nucleon-Nucleon Scattering Experiments

A brief review of different polarization experiments one can conduct with a pair of nucleons and of the associated experimental parameters will best help to identify the parameter $C_{NN}(\theta)$, measured in this experiment, in the proper perspective. The discussion is summarized in Table I. Whether the incoming particles are polarized or not, the outgoing particles are considerably polarized at almost all scattering angles.

(a) The simplest possible experiment would be a differential cross-section measurement with unpolarized beam and unpolarized target. The parameter measured is simply $I_0(\theta)$.

(b) The first step of sophistication is the classical double-scattering experiment. Here one adds the measurement of the component of polarization perpendicular to the plane of scattering of one of the

Table I. Summary of polarization experiments and associated parameters in elastic proton-proton scattering. A few more parameters appear for proton-neutron scattering where one needs to subscript the (X) in some cases.

X: one particle's polarization measured

*: related by time reversal

Initial State	Final State	Parameter Measured
-	-	I_0
X	-	P (*)
-	X	P (*)
X	X	D,R,A,R', or A'
X X	-	C_{NN} or C_{KP} (*)
-	X X	C_{NN} or C_{KP} (*)

four particles involved in the main interaction. (Clearly only two particles are involved, but referring to them as four particles helps to distinguish between incoming and outgoing states connected by time reversal, particularly since the two particles may themselves be indistinguishable in either the incoming or outgoing states.) There are two ways of conducting these double-scattering experiments related by time inversion. One may either polarize an initial-state particle by some means such as a first (polarizing) scattering of the beam prior to the main interaction and measure the differential cross section for each of two different incident-particle polarizations (typically equal in magnitude but opposite in sign), or one may obtain the polarization of one final-state particle by following the main scattering with a second (analyzing) scattering at each of two angles opposite to each other. Either way, one obtains a pair of differential cross sections whose sum is proportional to $I_0(\theta)$ and difference to $P(\theta)$, the "polarization" parameter. Note that the term "polarization parameter" is used interchangeably for all of the spin-associated parameters described here, as well as more specifically for this $P(\theta)$. If one postulates time-reversal invariance of the strong interaction, one expects identically the same value for the parameter measured in each of these two ways. With sufficient accuracy these double-scattering experiments may therefore furnish information about the magnitude of the coefficients of the scattering-matrix amplitudes that violate time-reversal invariance.

Next we describe the experiments classically referred to as "triple

scattering", in which one obtains the differential cross section as well as information about the polarization of two of the four particles involved. They naturally divide into two distinct categories:

(c) If the polarization is measured for an incoming and an outgoing particle, one obtains, depending on the components of polarization involved, the "depolarization" parameter $D(\theta)$, or the "rotation" parameters $R(\theta)$, $R'(\theta)$, $A(\theta)$, $A'(\theta)$, not all independent. Since the experiment is its own time inverse, these parameters furnish no information about time reversal invariance.

(d) If, on the other hand, the polarization is measured for both incoming or both outgoing particles simultaneously, one measures, depending again on the components of polarization involved, the "correlation" parameters $C_{NN}(\theta)$, $C_{KP}(\theta)$, etc. In principle we would again be testing time reversal invariance if we could compare the correlation parameters obtained separately from initial-and final-state polarizations.

Schumacher and Bethe[4] refer to the parameters of (c) as the components of the "depolarization" and the "polarization-transfer" tensors, while those in (d) make up the "polarization-correlation" tensor.

There are more categories than these with progressively less well-known parameters which are correspondingly more difficult to measure. We may, however, stop here, since we have clarified how C_{NN} fits into the scheme of possible experiments and that it may be measured in two different ways connected by time reversal. Unfortunately C_{NN} is a parameter that is not suitable for checking time-reversal invariance. In Appendix B we show that the time-reversal-invariance-violating amplitudes of the

Table II. Other measurements of C_{NN} in elastic proton-proton scattering

Beam Energy (MeV)	C.M. Angle θ (Deg)	$C_{NN}(\theta)$	Reference
20	90	-0.91 ± 0.05	5a*
310	90	$+0.84 \begin{smallmatrix} + 0.10 \\ - 0.22 \end{smallmatrix}$	5b
320	90	$+0.75 \pm 0.11$	5c
382	90	$+0.416 \pm 0.084$	5d
400	60	$+0.82 \pm 0.47$	5e
	90	$+0.60 \pm 0.09$	
450	90	$+0.70 \pm 0.15$	5e
640	54	$+0.57 \pm 0.14$	5f
	72	$+0.65 \pm 0.15$	
	90	$+0.93 \pm 0.21$	

*This is the only previous experiment done with a polarized beam and a polarized target.

scattering matrix appear in identically the same way in the analytic expressions of C_{NN} corresponding to the two ways of measuring it. Table II lists other measurements of C_{NN}.

C. Polarization Experiments without and with a Polarized Target

Before polarized targets were available, one was restricted to experiments involving the measurement of the polarization of the final-state particles (one or both) only, by measuring the "left-right" scattering asymmetry. This statement is of course strictly true only for the correlation experiments listed under (d) in the last section, although it seems to apply to measurements of the polarization (b) as well, while it is patently false for the parameters under (c).

The limitations under which one must work in this experimental arrangement are worthy of enumeration. The chief problems center around guarding against false asymmetries of all kinds and fighting low counting rates due to an extra scattering and, at low energies, low analyzing power. The false asymmetries may arise from these sources: asymmetrical beam intensity pattern across the second-scattering target, asymmetrical background counting rate, asymmetrical counter sensitivity due to presence of asymmetrical magnetic fields or to misallignment. None of these serious problems remain when a polarized target is used.

In addition to vanishing at low energy, the analyzing power is troublesome in its often unpredictable energy dependence at high energies. In the laboratory system the particles scattering at the main target come off at various energies, depending on the scattering angle. One therefore needs to know the analyzing power of the second-scattering target material as a function of energy, which means in most cases that one

needs to measure it independently.

Another consideration is the second-scattering detector arrangement. It is necessarily bulky and makes careful scattering-angle reversals difficult. Far more serious however is the great difficulty with which more than one second scattering can be handled at one time. In practice one mounts the counter telescopes that serve to count particles scattered by the second target on pivots centered on the second target. To jockey several of these telescopes associated with several second targets past each other in a reversal is clearly troublesome. One therefore finds oneself restricted to analyzing at one angle or possibly two angles of opposite sign, especially in analyzing the component of polarization perpendicular to the plane of scattering as in the case of C_{NN}. Moreover, this problem is closely coupled to one mentioned previously, since shifting objects such as other counters near the scattering centers most certainly affects the (cave) background somewhat. (Recently carbon-sandwich spark chambers have been used with great success to cover wider angular regions in second scatterings.[6] However this method suffers from analyzing-power variations to which we alluded above.) Further not-so-obvious limitations will be brought out in connection with the advantages of the polarized target as used in this experiment, which we discuss next.

The target we used was developed several years ago by Chamberlain, Jeffries, Schultz, and Shapiro[7] based on a much smaller model built by Jeffries.[8] The polarizing process is called "dynamic polarization". It produces high polarizations of the free protons in the waters of hydration of Nd^{142}-doped lanthanum magnesium nitrate crystals by exciting certain forbidden magnetic-dipole transitions involving both the paramagnetic

neodymium ions and the water protons. The necessary environment consists of an extremely uniform high magnetic field, a temperature of the order of $1^{\circ}K$, and a flood of microwave radiation of considerable power. The equipment which produces this environment is obviously much bulkier than a counter telescope (the magnet alone weighs 9 tons), but it doesn't have to be shifted during the asymmetry measurements.

The more obvious advantages of using the polarized target are:

(a) The number of scatters required to measure a given polarization parameter is reduced by one. For example triple-scattering experiments become double-scattering experiments, since the method of polarizing does not depend on the strong interaction. Thereby one obviously gains in overall flux, although perhaps not as much as might be hoped because of the small counters with which one must work for reasons to be discussed later.

(b) The polarization is high, limited by experimental technique and money rather than a constant of nature, and completely independent of energy.

(c) The polarization is reversed without a geometry change. One simply tunes the microwave generator to a slightly different frequency, thus exciting a different set of forbidden transitions in the crystals.

(d) One may experiment at any number of angles at once, limited only by target structure and the momentum of the slow outgoing particles, as discussed later.

(e) One can measure the polarization and correlation parameters in two different ways distinguished by time reversal.

Clearly the simplest proton-proton scattering experiment with a polarized target is to measure the differential cross section with an unpolarized beam for each of two opposite target polarizations. In this case, one measures $P(\theta)$. A pair of such experiments has recently been completed using our target.[9]

The first step of sophistication consists of enhancing one or the other component of beam polarization by some means such as a first scattering. Thus by polarizing the beam, and without any other changes, one measures the correlation parameters.

Indeed using the experimental arrangement and associated electronics from the last $P(\theta)$ run and adding only the features that polarize the beam in a direction parallel to the target polarization (perpendicular to the plane of scattering) we were able to make the measurements which yielded values of the parameter $C_{NN}(\theta)$. It will become clear later why one actually obtains three other quantities at the same time, namely $P(\theta)$, $I_0(\theta)$ (a useless quantity, unless one takes considerable pains to normalize it), as well as the average beam polarization.

In summary, the only safe way to remove all ambiguities from the nucleon-nucleon phase shifts is to determine the complete scattering matrix experimentally at a number of energies. We have reminded the reader of the parameters that are the building blocks of the scattering matrix and of the experiments that determine them, and we have enumerated the advantages of using the polarized proton target in performing the

experiments. In the next chapter we use the popular spin formalism to arrive at the relation between the parameter $C_{NN}(\theta)$ and the measured cross sections. In the third chapter we describe the experimental apparatus and in the fourth chapter the analysis of the data and the results.

II. THE SPIN FORMALISM

In this chapter we sketch out the formalism which clearly presents the connection between the scattering matrix and experiment. We assume a familiarity with the basic concepts of quantum mechanics. It is our intention to present only those steps in the development without which the continuity to the final results would be in question. More exhaustive treatment should be sought in Reference (1) and elsewhere. Our development will be nonrelativistic. Stapp[3] has shown that the nonrelativistic treatment of spin components normal to the scattering plane is permissible since they are unaffected by the Lorentz transformation.

A. The Scattering Matrix

First we introduce the scattering matrix. In elastic scattering of spinless particles we write the final ("outgoing") state wave function U^o in terms of the initial-state wave function U^i and the scattered part in the familiar asymptotic form

$$U^o = U^i + f(\theta) \times (\text{r.p.}) . \qquad (1)$$

Here $f(\theta)$ is the scattering amplitude, θ is the center-of-mass-system scattering angle, and (r.p.) is defined by

$$(\text{r.p.}) = (\text{radial part}) = \frac{e^{ikr}}{r} ,$$

where k is the center-of-mass momentum divided by $\hbar$.

The wave functions are normalized so that the differential cross section I_o is given by

$$I_o(\theta) = |f(\theta)|^2 . \qquad (2)$$

The symbol I_o is reserved for "differential cross section, initial state unpolarized".

To introduce spin we transform Eq. (1) explicitly into a relation between spin-wave-function components by factoring the spin parts out of the wave functions. Let X^i represent the spin part of the initial state and X^o that of the final state.. In the case of nucleon-nucleon scattering these spin functions of the combined spin space are 4 component spinors. We may then express U^o and U^i as

$$U^o = u^o X^o , \qquad U^i = u^i X^i .$$

The definitions of u^o and u^i are obvious. Equation (1) becomes

$$u^o X^o = u^i X^i(\phi) + X^f(\theta,\phi) \times (\text{r.p.})$$

where X^f if the scattered-(final-)part spin wave function which one expresses in terms of the initial-state spin function through the scattering matrix $M(\theta,\phi)$

$$X^f(\theta,\phi) = M(\theta,\phi)X^i(\phi) \qquad (3)$$

and ϕ is the azimuthal angle about the incident-particle momentum.

For pion-nucleon scattering in a given total-isotopic-spin state the M matrix is a 2×2 operator in spin space that has the familiar form

$$M(\theta,\phi) = g(\theta) + h(\theta)\vec{\sigma}\cdot\hat{N} \qquad (4a)$$

in terms of the Pauli spin matrices σ_x,σ_y, and σ_z and the unit normal to the scattering plane $\hat{N}$. For nucleon-nucleon scattering in a given isotopic-spin state the parity-conserving, time-reversal-invariant M matrix has in Wolfenstein's "single-particle" representation[2] the somewhat more complicated form

$$M(\theta,\phi) = B(\theta)S + C(\theta)(\sigma_{1N}+\sigma_{2N}) + N(\theta)\sigma_{1N}\sigma_{2N} + \frac{1}{2}G(\theta)(\sigma_{1P}\sigma_{2P}+\sigma_{1K}\sigma_{2K}) \quad (4b)$$
$$- \frac{1}{2}H(\theta)(\sigma_{1P}\sigma_{2P}-\sigma_{1K}\sigma_{2K})\,T$$

Here S and T are singlet and triplet projection operators respectively, B, C, N, G, and H are the theta-dependent Wolfenstein amplitudes, and the rest of the objects are 4×4 matrices composed of the Pauli spin matrices and the configuration-space vectors one associates with the interaction, e.g. $\sigma_{1N} = \vec{\sigma}_1 \cdot \hat{N} I_2$, in which I_2 is the identity operator for the spin state of particle 2.

These vectors are defined in terms of the center-of-mass momentum of the beam particle before and after the interaction, $\vec{k}_1$ and $\vec{k}_3$, respectively. One has $\hat{N}$ as the direction normal to the scattering plane together with three convenient directions in the scattering plane as follows

$$\hat{N} = \frac{\vec{k}_1 \times \vec{k}_3}{|\vec{k}_1 \times \vec{k}_3|} \qquad \hat{K} = \frac{\vec{k}_1 - \vec{k}_3}{|\vec{k}_1 - \vec{k}_3|}$$

$$\hat{P} = \frac{\vec{k}_1 + \vec{k}_3}{|\vec{k}_1 + \vec{k}_3|} \qquad \hat{S} = \frac{\hat{N} \times \vec{k}_1}{|\hat{N} \times \vec{k}_1|} \,.$$

$\hat{P}$ and $\hat{K}$ nonrelativistically point in the directions of the scattered and recoil particles, respectively, in the laboratory system while $\hat{S}$ is also in the scattering plane, but perpendicular to the beam on the side of the scattered beam particle.

Together with these vectors in configuration space we need to define some 4×4 spin matrices such as $\sigma_{1N}\sigma_{2N}$ which are perhaps best introduced

by analogy to the equivalent 2 x 2 matrices of the pion-nucleon system. Any operator in that system's spin space can be composed of three linearly independent, traceless, Hermitian 2 x 2 matrices together with the unit matrix in linear superposition. The three matrices are the Pauli spin matrices. For example the scattering matrix M is an operator in this spin space and is expressed in terms of the basic matrices as shown for pion-nucleon scattering in Eq. (4a). (The symbol for the unit matrix should appear next to $g(\theta)$.)

It is in fact possible to associate the same set of four basic matrices with each of the two particles of spin 1/2 involved in nucleon-nucleon scattering in order to make up the 16 basic matrices needed for the product spin space of that system. We subscript them with 1 and 2 remembering that set 1 operates only on particle 1 spinors and vice versa. This explains the notation rather well while one in practice often does computations with product space algebra to avoid confusion. The 16 matrices are signified by

$$I,\ \sigma_{i1}(3),\ \sigma_{i2}(3),\ \sigma_{i1}\sigma_{j2}(9)\ . \qquad (5)$$

One obtains the number of matrices of a given type shown in parentheses as one lets i and j range over x, y, and z. Note that the symbol I is used for unit matrix as well as cross section with initial state polarization. Moreover we have avoided writing as well as subscripting the unit matrix as is customary, realizing that "σ_{x1}" really means "$\sigma_{x1}I_2$" etc.

As shown in Appendix A the components of the composite state spinor X in Wolfenstein's "single particle" representation are related to the

components of the single particle spinors r and s through the relation

$$r_a \times s_b = X_{2(a-1)+b}$$

The subscripts a and b range over 1 and 2 while the subscript of X runs from 1 to 4. Similarly the prescription for writing down components of the product space matrices in terms of the Pauli spin matrices' components is

$$(\sigma_{i1})_{a,b} \times (\sigma_{j2})_{c,d} = (\sigma_{i1}\sigma_{j2})_{2(a-1)+c,\ 2(b-1)+d} .$$

As an example we give the expression for the composite state spinor of 2 nucleons both spinning parallel to the z axis in the representation where σ_z is diagonal.

Here $r = \begin{pmatrix}1\\0\end{pmatrix}$, $s = \begin{pmatrix}1\\0\end{pmatrix}$, and therefore $X = \begin{pmatrix}1\\0\\0\\0\end{pmatrix}$.

If the spin of particle 2 were reversed, we would find $X = \begin{pmatrix}0\\1\\0\\0\end{pmatrix}$.

The matrices listed in (5) are still not quite in the form shown in Eq. (4b). To arrive at the latter we have to introduce certain direction cosines designed to relate the arbitrary representation of the Pauli spin matrices (by which one for instance declares σ_z diagonal) to the laboratory. One therefore writes in a manner similar to $\vec{\sigma}\cdot\hat{N}$ of Eq. (4a)

$$\sigma_{1N}\sigma_{2N} = (\vec{\sigma}_1\cdot\hat{N}) \times (\vec{\sigma}_2\cdot\hat{N}) \ , \text{ etc.}$$

B. The Density Matrix

So far we have gone from scattering amplitude $f(\theta)$ to scattering matrix $M(\theta,\phi)$ and presented the form M takes for pion-nucleon and

nucleon-nucleon scattering in Wolfenstein's single-particle representation. Now it remains to relate the scattering matrix to observables in a manner similar to Eq. (2). However in doing this we are faced with considerable complications, since the states we are describing, such as beam and target, represent an incoherent mixture of pure spin states, although each particle by itself may be considered to be in a pure spin state. To properly combine the various amplitudes of the scattering matrix into expressions for observables such as polarization, one resorts to the density matrix formalism.

Quite generally let the set of spin states Y_i represent a basis of system normalized states for the n dimensional spin space of interest, $i = 1,2,\ldots n$. Each Y_i has n components $(Y_i)_j$, $j = 1,2,\ldots n$. Similarly let X represent a pure spin state. By the principle of superposition we may expand X in terms of the Y_i

$$X = \sum_{i=1}^{n} a_i Y_i$$

where a_i are complex coefficients. Any operator Q has expectation value $\langle Q \rangle$ in the state X given by

$$\langle Q \rangle = \langle X|Q|X \rangle = \sum_i a_i^* \sum_j a_j \langle Y_i|Q|Y_j \rangle = \sum_{i,j} a_i^* a_j q_{ij} \qquad (6)$$

where $q_{ij} = \langle Y_i|Q|Y_j \rangle$ is the appropriate matrix element of Q in terms of the basis representation.

The most arbitrary state would be an incoherent mixture of pure states like X, each called X_k, $k = 1,2,\ldots n$. Any operator Q has expectation value $\overline{\langle Q \rangle}$ in this arbitrary state given by

$$\overline{\langle Q \rangle} = \sum_{k=1}^{n} \omega_k \langle Q \rangle_k \qquad (7)$$

where the ω_k are the weight factors of the various pure states and each $\langle Q \rangle_k$ is of the form shown in Eq. (6) with the coefficients subscripted with k. Interchanging summation we finally arrive at

$$\overline{\langle Q \rangle} = \sum_k \omega_k \sum_{i,j} (a_k)_i^* (a_k)_j \, q_{ij} = \sum_{i,j} q_{ij} \sum_k \omega_k (a_k)_i^* (a_k)_j \; . \qquad (8)$$

We now define the density matrix ρ_k for the pure state X_k by the component equation

$$(\rho_k)_{ji} = (a_k)_i^* \, (a_k)_j$$

or equivalently by

$$\rho_k = X_k X_k^\dagger \, , \qquad (9)$$

where $X_k^\dagger$ is the row matrix adjoint to the column matrix X_k. Furthermore the density matrix ρ for the arbitrary incoherent mixture of the pure states is

$$\rho = \sum_{k=1}^{n} \omega_k \rho_k \; . \qquad (10)$$

In terms of ρ Eq. (8) becomes

$$\overline{\langle Q \rangle} = \sum_i \sum_j q_{ij} \rho_{ji}$$

$$\overline{\langle Q \rangle} = \mathrm{Tr}\, Q\rho \, , \qquad (11)$$

where Tr is the familiar contraction of "trace".

We are now ready to relate the final-state density matrix to the initial-state density matrix through the scattering matrix. As already pointed out at the beginning it is convenient to normalize the wave functions for the case of spinless particles so that the differential cross section is given by Eq. (2). In a like manner we normalize the spinor X_k^i in the case of the incident pure spin state so that

$$X_k^{i\dagger} X_k^i = 1 ,$$

for then the differential cross section $I(\theta,\phi)$ is given by

$$I = X^{f\dagger} X^f \tag{12}$$

where X_k^f is the final-state spinor.

The density matrix for the initial state is

$$\rho_k^i = X_k^i X_k^{i\dagger} ,$$

while the final-state spinor X_k^f is given according to Eq. (3) by

$$X_k^f = M X_k^i$$

and its density matrix is

$$\rho_k^f = X_k^f X_k^{f\dagger} = MX_k^i (MX_k^i)^\dagger = MX_k^i X_k^{i\dagger} M^\dagger$$

$$\rho_k^f = M \rho_k^i M^\dagger .$$

This expression applies to a mixed as well as to a pure spin state. We can see that when we use Eq. (10) and note that the scattering matrix is independent of k. For then we have

$$\rho^f = \sum_k \omega_k \rho_k^f = \sum_k \omega_k M \rho_k^i M^\dagger = M\Big(\sum_k \omega_k \rho_k^i\Big) M^\dagger = M \rho^i M^\dagger . \tag{13}$$

Using the relation

$$A^\dagger A = \mathrm{Tr}\, AA^\dagger$$

we find from Eqs. (12) and (13) that

$$I(\theta,\phi) = \mathrm{Tr}\, \rho^f = \mathrm{Tr}\, M\, \rho^i\, M^\dagger \quad . \tag{14}$$

In practice one often ignores the normalization of the initial-state density matrix. But then it is necessary to divide the observables by $\mathrm{Tr}\, \rho^i$. As an example Eq. (14) becomes

$$I(\theta,\phi) = \frac{\mathrm{Tr}\, \rho^f}{\mathrm{Tr}\, \rho^i} = \frac{\mathrm{Tr}\, M\, \rho^i\, M^\dagger}{\mathrm{Tr}\, \rho^i} \quad . \tag{14a}$$

We would like to introduce another form of the density matrix which is particularly suited for expressing the initial state. Since the density matrix is an operator in the composite spin space it can be expanded in terms of the set of basic Hermitian matrices listed in (5) which we now collectively call Q_μ . The property these matrices have in common which has not yet been mentioned is, for two particles of spin 1/2,

$$\mathrm{Tr}\, Q_\mu\, Q_\nu = 4\, \delta_{\mu\nu} \quad .$$

The proposed expansion is

$$\rho = \sum_\nu A_\nu\, Q_\nu \quad .$$

To evaluate the coefficients A_ν we operate on each side of this expression with Q_μ , take the trace, and get

$$\mathrm{Tr}\, Q_\mu\, \rho = \sum A_\nu\, \mathrm{Tr}\, Q_\mu\, Q_\nu$$

$$= 4\, A_\mu \quad .$$

But using Eq. (10) for arbitrary normalization of ρ we also have

$$\mathrm{Tr}\ Q_\mu\ \rho = \langle Q_\mu \rangle\ \mathrm{Tr}\ \rho$$

whence

$$A_\mu = \frac{\mathrm{Tr}\ \rho}{4} \langle Q_\mu \rangle$$

and therefore, specifically for the initial state,

$$\rho^i = \frac{\mathrm{Tr}\ \rho^i}{4} \sum_\mu \langle Q_\mu \rangle^i\ Q_\mu \ . \tag{15}$$

C. Application to $C_{NN}(\theta)$

We now apply this formalism to calculate a number of average values all related to our final expression involving C_{NN}. First of all we compute differential cross section I_0 and a few other observables for unpolarized beam and unpolarized target using Eq. (15). The only nonvanishing $\langle Q_\mu \rangle^i$ is $\langle I \rangle^i$, giving us for ρ^i

$$\rho^i = \frac{\mathrm{Tr}\ \rho^i}{4} \langle I \rangle^i\ I$$

Then Eq. (13) gives the final state density matrix as

$$\rho^f = M\ \rho^i\ M^\dagger = \frac{\mathrm{Tr}\ \rho^i}{4} \langle I \rangle^i\ M\ M^\dagger$$

and $I_0(\theta)$ is

$$I_0 = \frac{\mathrm{Tr}\ \rho^f}{\mathrm{Tr}\ \rho^i} = \frac{1}{4} \langle I \rangle^i\ \mathrm{Tr}\ M\ M^\dagger \ . \tag{16}$$

(We keep track of the $\langle I \rangle^i$ to show that they cancel in the final expression.) For the same initial state the final-state polarization of particle 3 is $P_1(\theta) = \langle \sigma_{1N} \rangle^f$ while that of particle 4 is $P_2(\theta) = \langle \sigma_{2N} \rangle^f$, given by

$$P_1 = \frac{\mathrm{Tr}\ \sigma_{1N}\ \rho^f}{\mathrm{Tr}\ \rho^f} = \frac{1}{4}\ \frac{\mathrm{Tr}\ \rho^i}{\mathrm{Tr}\ \rho^f}\ \langle I\rangle^i\ \mathrm{Tr}\ \sigma_{1N}\ M\ M^\dagger$$

$$P_1 = \frac{1}{4I_0}\ \langle I\rangle^i\ \mathrm{Tr}\ \sigma_{1N}\ M\ M^\dagger \qquad (17)$$

$$P_2 = \frac{1}{4I_0}\ \langle I\rangle^i\ \mathrm{Tr}\ \sigma_{2N}\ M\ M^\dagger . \qquad (18)$$

The correlation parameter C_{NN} is defined by $C_{NN}(\theta) = \langle \sigma_{1N}\sigma_{2N}\rangle^f$ for this case of the unpolarized particles in the initial state. It is given by

$$C_{NN} = \frac{1}{4I_0}\ \langle I\rangle^i\ \mathrm{Tr}(\sigma_{1N}\sigma_{2N})M\ M^\dagger . \qquad (19)$$

Now let us consider another experiment, one in which both initial state particles are polarized in a direction normal to the scattering plane. Let the respective polarizations be P_B for the beam particles and P_T for the target particles. Then the non-vanishing $\langle Q_\mu\rangle^i$ are the four quantities $\langle I\rangle^i$, $\langle \sigma_{1N}\rangle^i = P_B\langle I\rangle^i$, $\langle\sigma_{2N}\rangle^i = P_T\langle I\rangle^i$, and $\langle \sigma_{1N}\sigma_{2N}\rangle^i = P_BP_T\langle I\rangle^i$, which lead to the density matrix

$$\rho^i = \frac{\mathrm{Tr}\ \rho^i}{4}\left[1 + P_B\sigma_{1N} + P_T\sigma_{2N} + P_BP_T\sigma_{1N}\sigma_{2N}\right]\langle I\rangle^i .$$

For this experimental arrangement the differential cross section is given by

$$I(\theta) = \frac{\mathrm{Tr}\ \rho^f}{\mathrm{Tr}\ \rho^i}$$
$$= \frac{1}{4}\Big[\mathrm{Tr}\ M\ M^\dagger + P_B\ \mathrm{Tr}\ M\sigma_{1N}\ M^\dagger + P_T\ \mathrm{Tr}\ M\sigma_{2N}\ M^\dagger +$$
$$+ P_BP_T\ \mathrm{Tr}\ M\sigma_{1N}\sigma_{2N}\ M^\dagger\Big]\langle I\rangle^i .$$

This expression becomes

$$I(\theta) = I_0(\theta)\left[1 + P_B P_1(\theta) + P_T P_2(\theta) + P_B P_T\, C_{NN}(\theta)\right]$$

provided we can show that the following relations hold

$$\mathrm{Tr}\ \sigma_{1N}\, M\, M^{\dagger} = \mathrm{Tr}\ M\, \sigma_{1N}\, M^{\dagger} \tag{21}$$

$$\mathrm{Tr}\ \sigma_{2N}\, M\, M^{\dagger} = \mathrm{Tr}\ M\, \sigma_{2N}\, M^{\dagger} \tag{22}$$

$$\mathrm{Tr}\ \sigma_{1N}\sigma_{2N}\, M\, M^{\dagger} = \mathrm{Tr}\ M\, \sigma_{1N}\sigma_{2N}\, M^{\dagger}\ . \tag{23}$$

If furthermore we recognize that $P_1(\theta) = P_2(\theta) = P(\theta)$ in the case of proton-proton scattering, where we are dealing with two identical particles, we finally have

$$I(\theta) = I_0(\theta)\left[1 + (P_B + P_T)P(\theta) + P_B P_T C_{NN}(\theta)\right]\ . \tag{24}$$

This is the equation we shall use in the analysis of our data in Chapter IV. Regarding Eqs. (21-23) we note that Betz[9b] has verified expressions (21) and (22) provided the time-reversal invariance violating terms of the scattering matrix vanish. He uses only the commutation relations of the Pauli spin matrices and the properties of their traces. Using the same techniques as Betz we show in Appendix B that Eq. (23) holds whether the time-reversal invariance violating amplitudes vanish or not.

III. EXPERIMENTAL APPARATUS

A. Polarized-Proton Beam

1. Physical Description

The geometry of the polarized target used in this experiment is such that the orientation of the scattering plane is vertical. The target is polarized horizontally and perpendicular to the scattering plane. To measure C_{NN} we have polarized the beam horizontally by a first scattering in the vertical plane. Unpolarized protons extracted from the 184-in. cyclotron at fixed energy (nominally 740 MeV) are collimated by a set of 4-in. brass jaws of the pre-magnet collimator, bent into the proton cave direction by the steering magnet, and passed through an 8-in.-bore quadrupole doublet focusing magnet that focuses the protons at the first scattering target in the proton cave. From here on the system is shown in Fig. 1.

The protons emerge from the evacuated beam tube and enter the proton cave. Here the beam is deflected by a pair of bending magnets to cross over its original trajectory at an angle of 12 deg at the position where the first scattering target is located. At this point the beam spot measures about 1.5 in. horizontally by 0.5 in. vertically. The beam's path through 6 in. of liquid hydrogen, viewed at an angle of 12 deg from the beam, then appears as a particle source about 1.5-in.-square. Before it buries itself in a beamstopper of 10 ft. of concrete, the beam passes through a split ion chamber to provide a signal for the experimenter as a check on the course of the beam.

Particles scattering elastically in the first target in the same

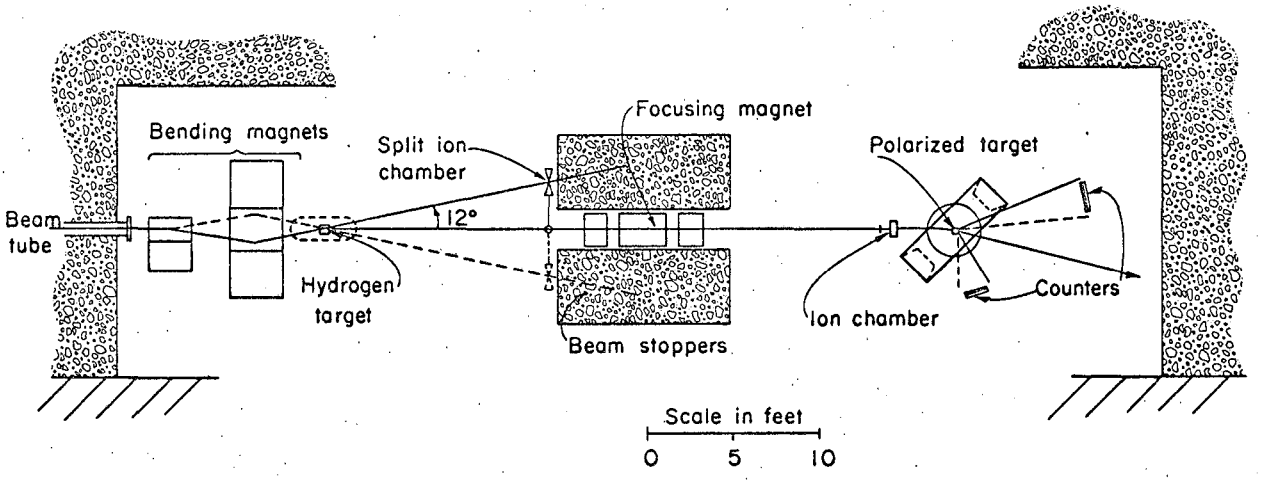

Fig. 1. Polarized-proton beam system. Protons from the 184-in. cyclotron enter from the left.

direction as the protons entering the cave from the cyclotron make up the polarized beam. They are focussed onto the polarized target crystals by an 8-in.-bore symmetric quadrupole triplet focussing magnet buried in the wall of shielding near the center of the cave. The beam stoppers are part of the same shielding wall. The magnification of this focusing magnet in both vertical and horizontal planes is about -1, giving a beam spot approximately 1.5-in.-square at the polarized target. A 2-in.-thick brass collimator with 4-in. by 6-in. oval opening, located in the first section of the focussing magnet, limits the solid angle of acceptance to about 6×10^{-4} sr. The range of scattering angles thus accepted from the first target is 12.1 ± 0.6 deg.

There is a 3 MeV energy variation across the second target in the plane of scattering arising from a small variation in the average angle of scattering across the source from 11.9 to 12.3 deg. The variation reverses with the beam polarization and is potentially a cause of a small false asymmetry. Its effect is to vary the width of the elastic-scattering distribution, but only in the plane of scattering. This elastic peak of the polarized target will be discussed in Section (B-3) of this chapter. Here we only mention that there is no cause for alarm as long as the whole peak region is included in the analysis of the data.

To reduce multiple scattering of the polarized-beam protons an 8-in.-diameter helium bag at 1 atm of pressure is used in the section of beam between the first-target vacuum jacket and the ionization chamber at the second target.

Range curve measurements of the polarized beam indicate a beam energy of 683 MeV.

2. Composition

Not all of the particles in the polarized beam interacting in the polarized target originate from elastic collisions in the hydrogen (EH) of the first target. There are two other principal sources of particles: elastic and diffraction scattering in non-hydrogen material (NH) such as flask domes, and inelastic scattering in hydrogen (IH).

It is necessary to consider the possible sources of beam contamination in some detail since the polarized beam does not contain the usual spectrometers to purify the momentum spectrum. Moreover, the range curve taken of the polarized beam gives the energy of the most abundant component of the beam, but it is not good enough to give detailed information about the spectrum.

The NH protons are of approximately the same energy as the EH protons. They constitute about 6% of all the particles arriving at the target as shown in the flask-empty rate and are not easily separated from the EH protons even in a beam of greater complexity. That the flask domes are the primary sources of NH protons can be seen as follows. The first scattering target is a 6-in.-long, 6-in.-diameter flask of liquid hydrogen (1.08 g/cm^2) with 0.005-in.-thick domes of aluminum (0.07 g/cm^2 total). The observed flask-empty - to - flask-full counting ratio of about 1:16 is rather similar to the ratio of the quoted target densities. The one other potential source of NH scatters is the hydrogen target vacuum jacket. By keeping the 0.035-in.-thick aluminum domes (0.5 g/cm^2 total) as much as 18 in.

upstream and downstream from target center, the sources represented by the intersections of the primary beam and the domes are kept 3.5 in. above and below the polarized-beam axis from where they can not be made to irradiate the polarized-target crystals of cross-sectional area 1-in.-square by a system of lenses of absolute magnification 1. The beam line through the first target is illustrated in Fig. 2.

IH protons are produced copiously at the first target. A glance at the shape of the proton-proton total cross section shows that between 300 and 700 MeV it doubles in value. 300 MeV is near the threshold for pion production. Since the elastic proton-proton cross section remains about constant above 300 MeV, the increase is due to inelastic events. This means that at an incident-particle kinetic energy of 740 MeV for every EH event there is an IH event in the first target. Moreover these IH protons in the laboratory system occur in a narrow cone in the forward direction with center-of-mass to laboratory solid angle conversion factors several times as large as for the EH protons. With the center-of-mass distributions about constant for both EH and IH events (we ignore the coulomb peak) we have several IH protons entering our solid angle defining collimator for each EH proton.

Clearly the focusing properties of the quadrupole magnet are such that the IH protons rapidly run out of phase space with lower momentum. In Table III we show how very dilute this IH component of the beam is at the polarized target, if we assume with Mandelstam[10] that near threshold pion production is dominated by Δ (1238) formation.

To explain the entries in Table III in some detail we follow through

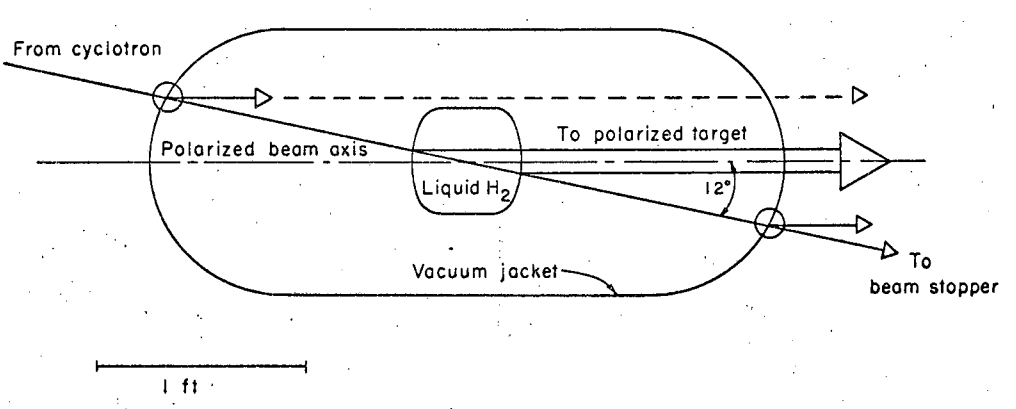

Fig. 2. Beam line through the first target and sources of polarized-beam protons.

Table III. Study of polarized-beam contamination due to Δ (1238) production in the first-scattering target.

	$p + p \rightarrow$	I_z	Clebsch-Gordan coefficients	Relative reaction rate (A)	Mean kinetic energy in polarized beam (MeV)					
					680	282	230	107	76	
					Number of protons yielded (B)					
I	$p + p$	$\frac{1}{2} + \frac{1}{2}$	-	1	2	-	-	-	-	I
II	$p + (p + \pi^o)$	$\frac{1}{2} + (\frac{1}{2} + 0)$	$\sqrt{\frac{2}{3}}$	$\frac{1}{6}$	-	1	1	1	1	II
III	$p + (n + \pi^+)$	$\frac{1}{2} + (-\frac{1}{2} + 1)$	$\sqrt{\frac{1}{3}}$	$\frac{1}{12}$	-	1	-	-	1	III
IV	$n + (p + \pi^+)$	$-\frac{1}{2} + \frac{3}{2}$	$\sqrt{\frac{3}{4}}$	$\frac{3}{4}$	-	-	1	1	-	IV
				Phase-space factor (C)	1	1.2×10^{-2}	2.9×10^{-3}	4×10^{-6}	2×10^{-7}	
				Solid-angle conversion factor (D)	5	17	30	13	4	
					Product of A, B, C, and D					
					10	-	-	-	-	I
					-	3.4×10^{-2}	1.5×10^{-2}	8.7×10^{-6}	1.3×10^{-7}	II
					-	1.7×10^{-2}	-	-	6.7×10^{-8}	III
					-	-	6.5×10^{-2}	3.9×10^{-5}	-	IV
				Polarized-beam constituents	1	5.1×10^{-3}	8.0×10^{-3}	4.8×10^{-6}	2×10^{-8}	

with the reaction called (II), namely

$$p + p \rightarrow p_1 + \Delta \rightarrow p_1 + p_2 + \pi^o .$$

From the Clebsch-Gordan coefficients involved we see that this reaction occurs 1/6 of the time an IH reaction occurs. (Note that the sum of the IH reaction rates by assumption equals the EH rate.) If we count the total number of protons this reaction yields and classify them by their energy at 12 deg in the laboratory system we find that the proton marked p_1 has either 282 MeV or 76 MeV depending on whether it is going forward or backward in the center-of-mass system while the one marked p_2 has energies centered near 230 or 107 MeV with variations that depend on the decay direction of the Δ. Taking into account the rate for the reaction, the correct center-of-mass-to-laboratory solid angle conversion factor for each of the beam components it yields, as well as the correct phase space of the polarized-target crystals at the source (first target) for the various particle momenta, we find the relative amounts of contamination at these various average momenta listed in the table.

The results of Table III are interpreted to mean that, to first order, the energy spectrum of the polarized beam contains a narrow line ($\frac{\Delta p}{p}$ about $\pm$ 1.5%, same as the primary cyclotron beam) of protons at 680 MeV of intensity 1, another at 282 MeV of intensity 5.1×10^{-3}, a broad line at 230 MeV of intensity 8.0×10^{-3}, etc. The total low-energy-proton contamination is therefore less than 1.5%.

The positive pions of reactions III and IV have a laboratory-system kinetic energy of about 150 MeV. Even if we allow them a solid

angle conversion factor similar to the protons, their momenta are so low in relation that they suffer from considerably less phase space than the slowest protons considered. The same argument applies to their decay products. Moreover, the kinematic requirements of the counter arrangements strongly discriminate against all reactions due to beam particles that are not protons.

3. Rates

Although no absolute flux determinations were made during the experiment, we give here the best estimates available. During the experiment the proton flux from the 184-in. was about 1.5×10^{11} particles/sec., a factor of two or more below maximum capable. It was thought best to clip the beam somewhat in order to keep the spot size at the first target and therefore at the polarized-target crystals small. The motivation is to minimize scattering off parts of the equipment surrounding the crystals. Moreover the intensity pattern of the beam spot at the crystals has to be as uniform as possible since only the average target-proton polarization can be measured reliably, while the target polarization is in fact not uniform, as shown by Betz. Clearly the polarization parameters cannot be measured well if one is dealing with a complicated intensity distribution across a non-uniformly polarized target. The clipping of the beam is necessary to achieve the combination of intensity distribution and spot size desired.

Using an incident flux of 1.5×10^{11} protons/sec, target density of 1 g/cm^2, solid angle of 6×10^{-4} sr., and differential cross section for elastic scattering in hydrogen of 40 mb/sr(lab) as measured by McManigal,

one arrives at a flux of about 3×10^6 EH protons/sec in the polarized beam. This number is in excellent agreement with the rate registered by the ion chamber in the beam near the polarized target. The ion-chamber rate is actually about three times higher, because it is sensitive to the protons from the NH sources in the first-target vacuum jacket as well as a considerable fraction of the IH protons and pion decay products that never reach the target crystals.

4. Beam Polarization

One of the numbers resulting from the data analysis is the average beam polarization. It is found to be 0.44 ± 0.02. This number represents the average polarization of the EH and NH particles and is not strictly speaking the parameter P(12 deg (lab)) for proton-proton scattering.

In order to avoid fluctuations of the beam polarization, i.e. deviations from the measured average, particularly during reversals, considerable care is exercised in reversing the first target scattering angle. The reversal is basically simple. One reverses the fields in the two bending magnets just upstream of the first target and relocates the split ion-chamber in front of the other beam stopper. The scattering angle is kept constant in magnitude by, first of all, maintaining the location of the polarized-beam source, i.e. the center-of-gravity of the unpolarized beam path through the first target. Since the solid-angle-defining collimator of the polarized beam remains fixed in the process, this also leaves the polarized beam axis fixed. Secondly, one needs to maintain the distance of the ion-chamber split from the axis. This is done by mounting it on a pivot centered on the beam

axis just upstream from the collimator. The only complications arise from the hysteresis in the bending magnets, which one needs to manipulate consistently.

We have reported on the features of the polarized beam in some detail since it promises further applicability. As has been shown, it combines constant high polarization with easy reversibility. Moreover, it has excellent momentum characteristics in spite of its simplicity, provided non-hydrogen scatterings are avoided at the first target.

B. Polarized-Proton Target

The second-scattering target used in this experiment has been described by Schultz.[7] We only summarize the salient features.

1. Dynamic Polarization

The target material consists of a stack of four single crystals of $La_2Mg_3(NO_3)_{12}\cdot 24H_2O$ in which a fraction of one percent of the La ions have been randomly replaced by Nd^{142} ions. In this material only the Nd ions are strongly paramagnetic and therefore readily polarized in an external magnetic field. Although they have a high spin quantum number, only two of their energy levels are significantly populated at an operating temperature of about $1^{\circ}K$. This behavior in a field resembles the electron's magnetic moment quantization, whence these paramagnetic ions are popularly called "electrons". We call the magnitude of their splitting in the external field H. $\Delta = g\mu_e H$,

g being their spectroscopic splitting factor and μ_e the Bohr magneton. A proton spin would similarly be quantized with energy splitting of $\delta = g_p \mu_p H$, μ_p being the nuclear magneton.

The four energy levels of an electron-proton pair in an external field H are shown in Fig. 3. There we see the various transitions corresponding to simultaneous spin flips labeled "allowed" or "forbidden" depending on their relaxation times. When the crystals are in equilibrium with the heat reservoir of the helium bath, whose boiling point is reduced from $4^{\circ}K$ to $1.3^{\circ}K$ by means of a mechanical pump, the relative populations of the four levels are given by Boltzman's statistics, as shown in the figure, resulting in a proton polarization P_T given by

$$P_T = \frac{\sum m_i \omega_i}{s \sum \omega_i} = \tanh \frac{\delta}{2kT}$$

Here ω_i is the relative population of the ith level, m_i the proton's spin projection, s its spin quantum number, k is Boltzman's constant, and T is the absolute temperature. In Fig. 3 M is the electron's spin projection on the field direction. When the crystals are flooded with microwaves whose photons have exactly the energy of one or the other forbidden transition, stimulated emission and absorption occurs tending to equalize the levels separated by the forbidden-transition energy. The new populations for one of these transitions are given in Fig. 3 under the heading "...when saturating $\Delta - \delta$", and the resulting polarization is

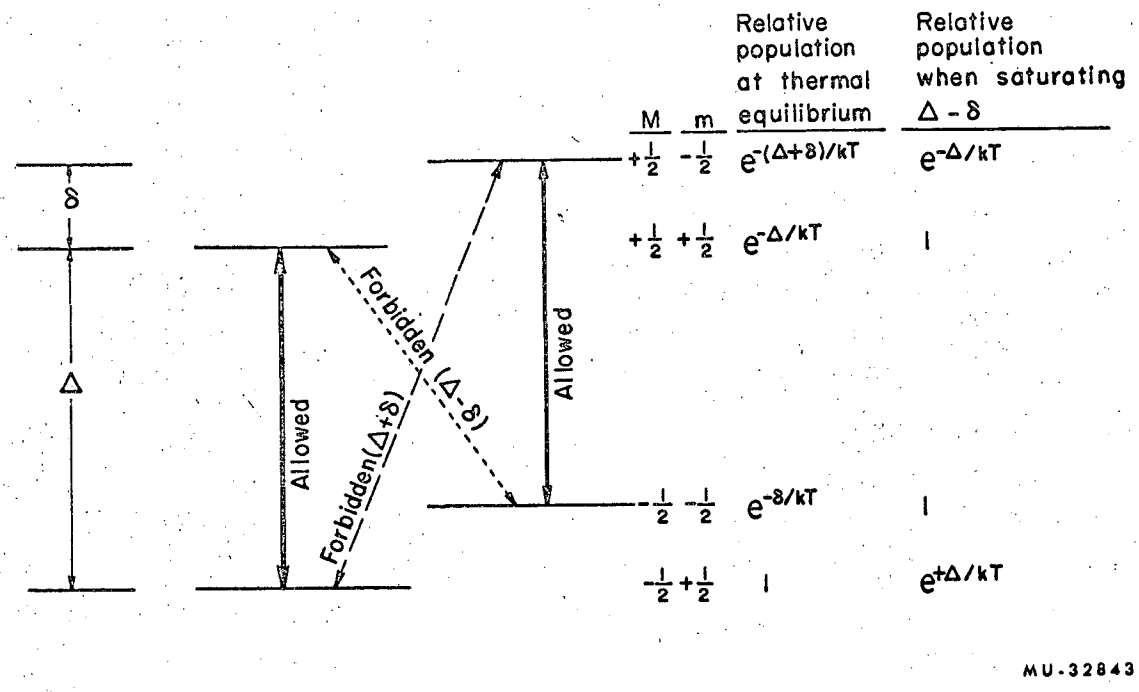

Fig. 3. Energy levels of an electron-proton system due to their magnetic moments in a magnetic field.

$$P_T = \tanh \frac{\Delta}{2kT} .$$

If one instead saturates the transition $\Delta + \delta$, P_T becomes

$$P_T = - \tanh \frac{\Delta}{2hT} .$$

This of course is an ideal maximum, since the power absorbed from the microwaves in the polarizing process tends to keep the temperature of the crystals above that of the helium bath by an unknown amount. Moreover, there is a multitude of reasons why it is practically impossible to saturate one of the forbidden transitions without at the same time pumping some small amount of power into the allowed transition thereby immediately depolarizing the sample to some extent.

2. Target Polarization Measurement

If this expression for the polarization were the only way to determine the target polarization one would be faced with tremendous uncertainty. Instead one resorts to "nuclear magnetic resonance" (NMR) techniques to measure the target polarization directly. Figure 4 shows the associated circuitry. We describe it as follows. The crystals are placed entirely into the sensitive volume of a small sensing coil which is the inductive part of a parallel resonant circuit driven by a constant-current variable-frequency rf oscillator at the frequency (or rather: through the spectrum of frequencies) of the δ-type transitions. Due to the imaginary part of their susceptibility the crystals add a resistive component (positive or negative) to the sensing coil's part of the parallel resonant circuit, absorbing or

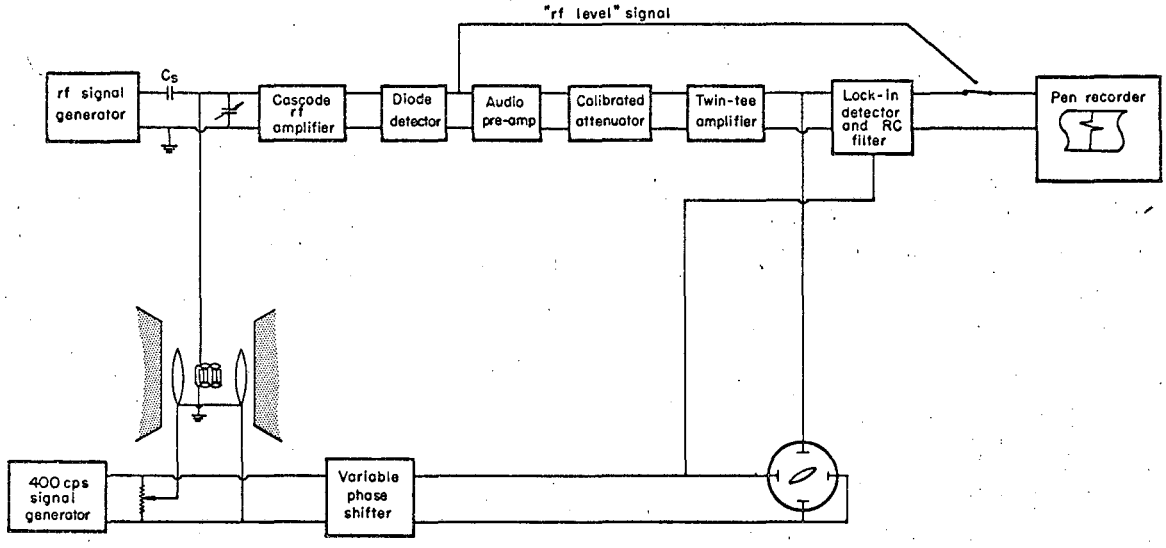

Fig. 4. Schematic diagram of the Q-meter detector. The 400 cps equipment shown at the bottom causes the differentiation of the NMR signal.

emitting more or less power as a fraction of frequency depending on the relative populations of the proton spin levels. In effect the crystals are changing the Q of the resonant circuit depending on the proton polarization, giving this type of circuit the name "Q-meter".

The procedure to determine the polarization is clear. One calculates the polarization assuming the crystals in thermal equilibrium (TE) with the temperature bath of known temperature (microwaves off) and calibrates the NMR detection system by ascertaining the resonance absorption curve corresponding to this reliable theoretical calculation. Then one polarizes by flooding the crystals with microwave power of suitable frequency to saturate one of the forbidden transitions. If one repeats the NMR curve, one measures a new area under the absorption curve (either positive or negative). The ratio of the new area to the TE area represents the enhancement factor which multiplies the calculated TE polarization to give the enhanced target polarization.

This basically simple procedure is in practice complicated by a variety of more or less tangible factors. The TE polarization depends critically on the temperature of the helium bath which it is difficult to measure. The detection system contains non-linearities which need to be considered in the area computations of the absorption curves. Moreover, although the target polarizations are proportional to these areas under certain ideal conditions, the limitations imposed by real conditions need to be properly understood.

3. Scattering, Non-Hydrogen Background

We have shown how it is possible to orient dynamically proton

spins by exciting certain forbidden transitions involving simultaneous spin flips with paramagnetic impurities. The protons one polarizes in this way are the hydrogen nuclei of the waters of hydration. In the $La_2Mg_3(NO_3)_{12}\cdot 24H_2O$ crystals these polarized protons comprise only 3% of the total crystal weight, or about 6% of the total crystal protons, bound or unbound. But they are the only unbound protons, and as a consequence one can identify kinematically the events due to the polarized protons.

The typical scattering situation is shown in Fig. 5. At the top of the figure we consider a series of scattering events in a crystal of the type we have described, but of infinitesimal size. We place a small proton counter at a fixed position and ask in which direction the conjugate protons are going. Those conjugate particles associated with reactions off the unbound (polarized) protons will come off in a unique direction, while those off the bound protons of the heavy nuclei will appear in a large three-dimensional bell-shaped distribution due to the Fermi motion of the target particles. If we increase the target size, the delta-function distribution of the free-proton events spreads out due to a multitude of effects coupled to the target size, while the other is essentially unchanged, as shown in the middle of the figure. The normalization of the distributions reflects the free-to-bound-proton ratio.

In order to arrive at pure free-proton counting rates one needs to determine the bound-proton background accurately. One does this in two steps. First one replaces the real crystals by a dummy target

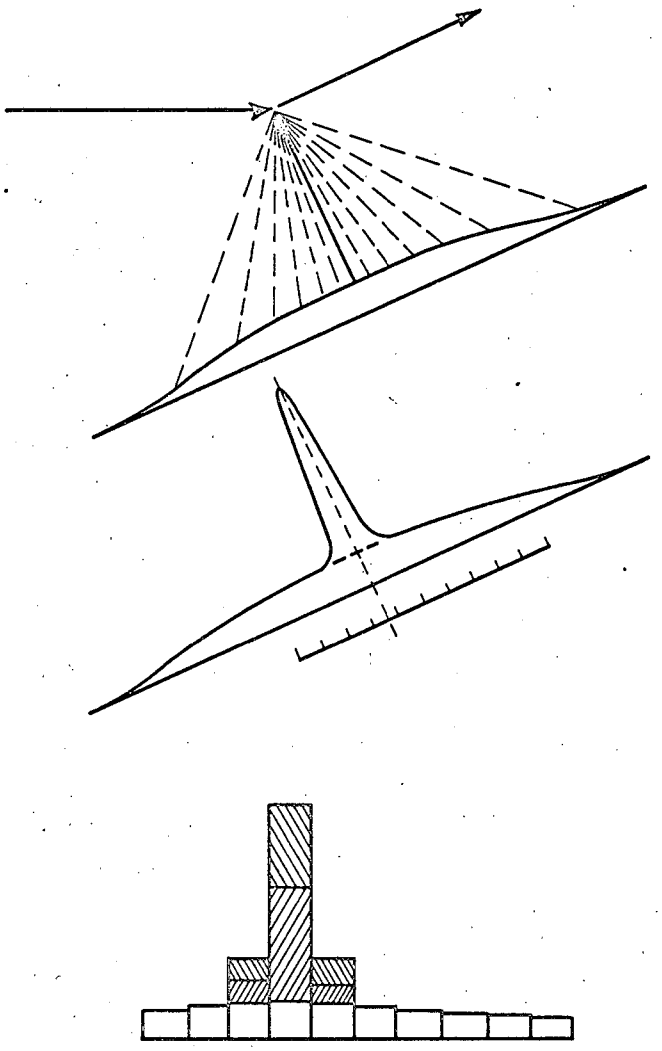

MUB-4824

Fig. 5. Conjugate particle distributions due to scattering from hydrogen and non-hydrogen target material.

Table II. Composition of the crystal and dummy target.

Crystal target (26.1 g of $La_2Mg_3(NO_3)_{12}\cdot 24H_2O$)				Dummy target (3.36 g of MgF_2, 6.70 g of $BaCO_3$, and 15.65 g of CF_2:CF_2(Teflon))			
Element	Atomic No.	Atomic weight	Total weight (g)	Element	Atomic No.	Atomic weight	Total weight (g)
La	57	138.9	4.7	Ba	56	137.4	4.7
Mg	12	24.3	1.3	Mg	12	24.3	1.3
N	7	14.0	2.9	C	6	12.0	4.2
O	8	16.0	16.4	O	8	16.0	1.6
				F	9	19.0	14.0
H	1	1.0	0.8	-	-	-	-

containing nearly the same materials as the crystals but no hydrogen. Certain substitutions are inevitable, e.g. nitrates are notoriously hygroscopic and must be avoided. In Table IV the composition of the dummy target used in this experiment is compared to that of the crystals. By scattering off the dummy target one gets the shape of the background distribution in the region of the free-proton distribution. Finally one normalizes this background distribution to compensate for differences in target densities by catching a good portion of the real crystal background distribution near the free-proton events.

The necessary conjugate-particle counter arrangement is shown in the middle of Fig. 5 with three possible distributions of relative counts shown at the bottom, for three different scattering situations: (a) dummy target only, (b) crystals, protons polarized one way, and finally (c) crystals, polarization reversed. With this type of detector arrangement one may impose strict requirements of coplanarity whereby one is sensitive to only a thin slice of the broad background distribution containing however all or most of the polarized hydrogen events. It has been possible to achieve hydrogen-to-background ratios of 10 to 1, e.g. by optimizing the beam spot and counter sizes, in spite of the overall 15 to 1 preponderance of the background events.

C. Counters and Electronics

The experiment is actually done with a pair of ten-counter arrays as shown in Fig. 6. The particles scattering left are the faster ones, going into the forward hemisphere in the center-of-mass system. They register in the up or α array, while the slower conjugate particles

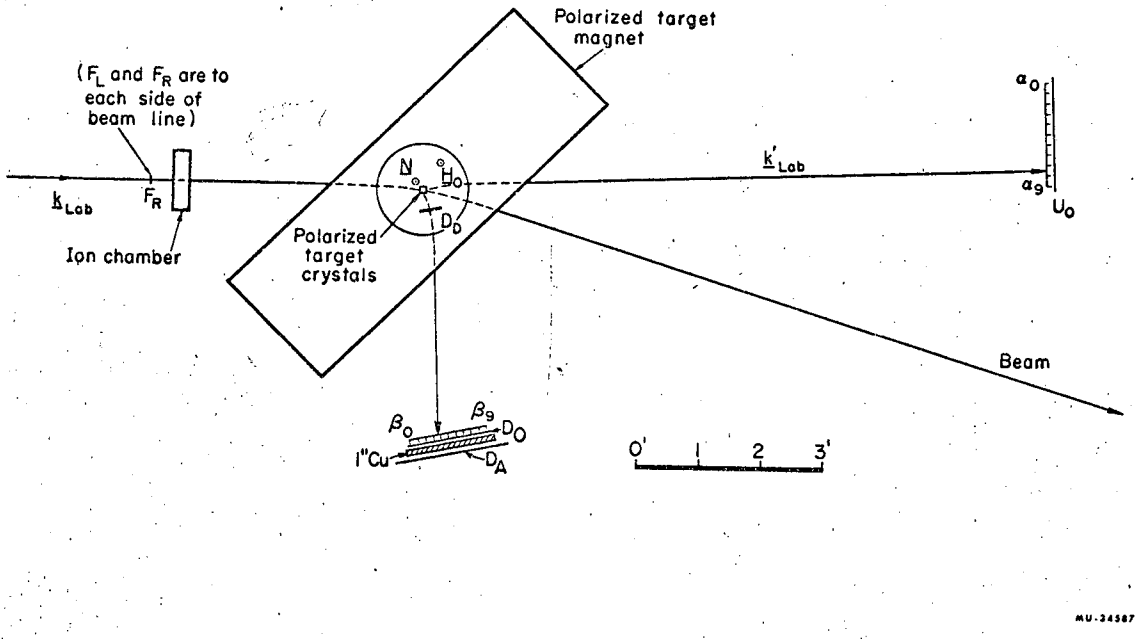

Fig. 6. Arrangement of the scintillation counters. The counter dimensions were:

α_i (2x1x1/2 in.) (ten counters)	U_o (22x3/2x1.2 in.)
β_j (3/2x3/2x1/2 in.) (ten counters)	D_D (4-1/4x3/2x1/8 in.)
E_1, E_2 (2x1x1/2 in.)	D_o (16x2x1/2 in.)
F_L, F_R (1/8x1/8x1/8 in.)	D_A (22x4-1/2x1/2 in.)

The direction of the normal to the scattering plane $\underline{N}$ and the direction of the external field $\underline{H}_o$ are indicated near the crystals. Since the proton has a positive magnetic moment, positive target polarization is parallel to $\underline{H}_o$.

find their way into the down or β array. Each one of the ten counters in the up array coupled with all ten counters of the down array represents a system of counters as described in the last section. For each up counter the hydrogen peak falls into a different combination of down counters.

The sizes of the individual counters and the distances of the counters from the target are governed by considerations of the hydrogen-to-background counting ratio, as well as expected counting rates. The width of the counters in the ϕ direction is fixed by requirements of coplanarity to include most of the hydrogen-peak distribution under good peak-to-background conditions. In practice this means that the width of the fast-particle array is about the width of the target, while that of the slow-particle array may be somewhat greater. The length of the counters in the theta direction allows some freedom. Again peak-to-background considerations enter in. If we consider what happens when we double the length of a fast-particle counter we find that both background and peak distributions of the conjugate particles double in normalization, but they both increase in width by one and the same amount corresponding to the theta increase of the fast-particle counter. Clearly this width change is insignificant for the background distribution while it doubles the width of the hydrogen peak. Essentially therefore the peak-to-background ratio has been cut in half by doubling the fast-particle counter length. In practice one keeps the fast-particle counter length near target size within a factor of 2, and fixes the length of the slow-particle counters to allow good resolution of the hydrogen peak, i.e. two or three counters to cover the peak

region. The total number of counters in each array is primarily dependent on the capabilities of the data storing logic.

One may sum up the counter size ideas by building the individual counters about the size of the target and adjusting their distances from the target so that they subtend an angle equal to the rms multiple-scattering angle. Moreover the sizes may be slightly adjusted so that the up and down counters subtend about the same solid angle in the center-of-mass system. The counters are sequentially numbered as shown in Fig. 6. Events corresponding to single coincidences between one up and one down counter (α_i , β_j) are counted in the appropriate element (i,j) of a 100-channel matrix of scalers. Each of the arrays is also covered by overlay counters U_o and D_o. Furthermore, to increase the hydrogen-to-background ratio a small counter D_D is placed near the target crystals thus eliminating background due to scattering off the heavy vacuum-jacket flanges and magnet pole pieces.

Figure 7 shows the schematic diagram of the event-processing logic. All α-counter signals are added to make SUMα , all β counters SUMβ. A coincidence of D_D , SUMβ , and D_o is called DOWN. A possible event is then signified by a coincidence of DOWN, SUMα, and U_o , which generates a storage trigger, STOT . If only one α and one β counter have fired, the appropriate memory address is generated and checked and, if correct, one count is stored in the corresponding matrix element. Otherwise the event is rejected.

D_A is a counter of the size of D_o , located behind it but separated

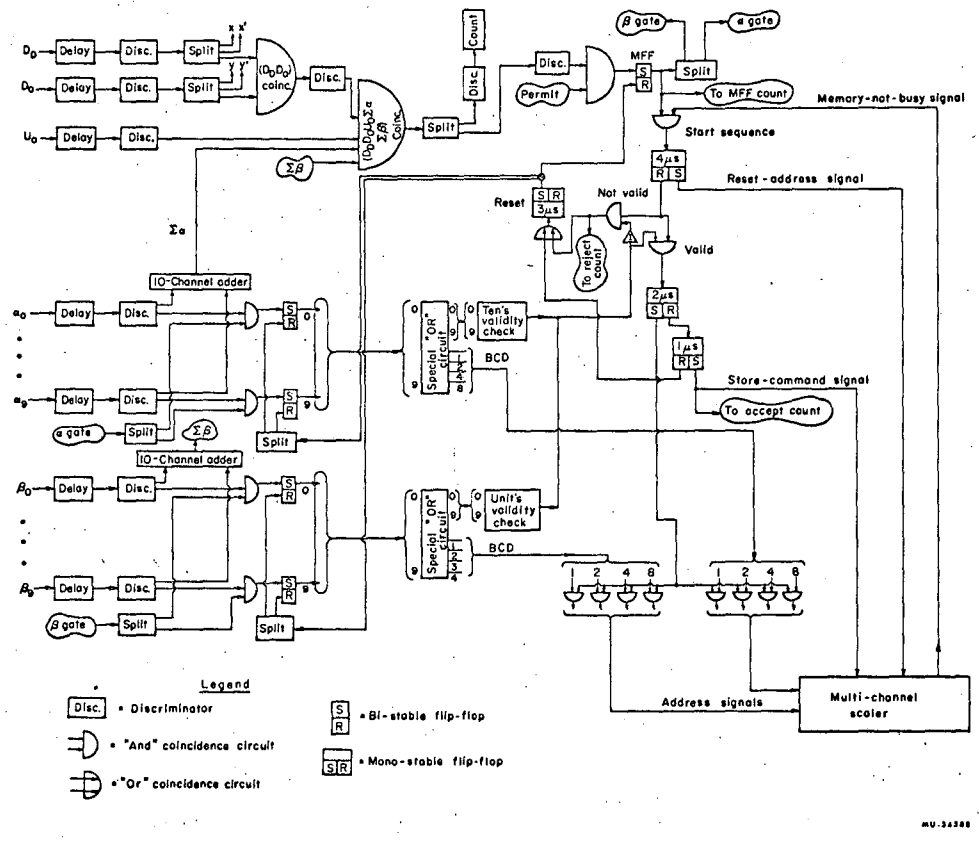

Fig. 7. Event-identifying and storing logic.

by a 1-in. slab of copper designed to keep the protons from events involving the free target protons from reaching D_A.

A number of monitors are incorporated to normalize the many data runs following numerous polarization reversals. The schematic diagrams of these and of a variety of data quality control devices are shown in Figs. 8 and 9. Of all the monitors the ionization chamber proves by far the most useful.

There are three quality control devices of significance. One is the beam-spill visual display of the integrated U_o singles rate. Another is a coincidence of D_D, D_o, and D_A with one of the signals purposely delayed by 53 ns, the time between cyclotron rf pulses, which registers the accidental rate in the undelayed coincidence of these signals. Both of these devices allow a continuous check on the crew's tuning of the cyclotron. The third is the split ion chamber. It is an ordinary ionization chamber with a split signal foil. In the way it is used it gives a very sensitive indication of shifts of the center of intensity of the primary proton beam by driving the pen of a zero-reading chart recorder. The pen motion may magnify beam motion several times. As a consequence one has a continuous indication of the current regulation in the two bending magnets just upstream from the first target which, if poor, would shift the location of the polarized-beam source. Moreover the split ion chamber is very useful in beam-polarization reversals. Instead of having to set two magnet currents with great care to reproduce the deflected beam line, one has to set one current carefully while the other is set to center the beam on the

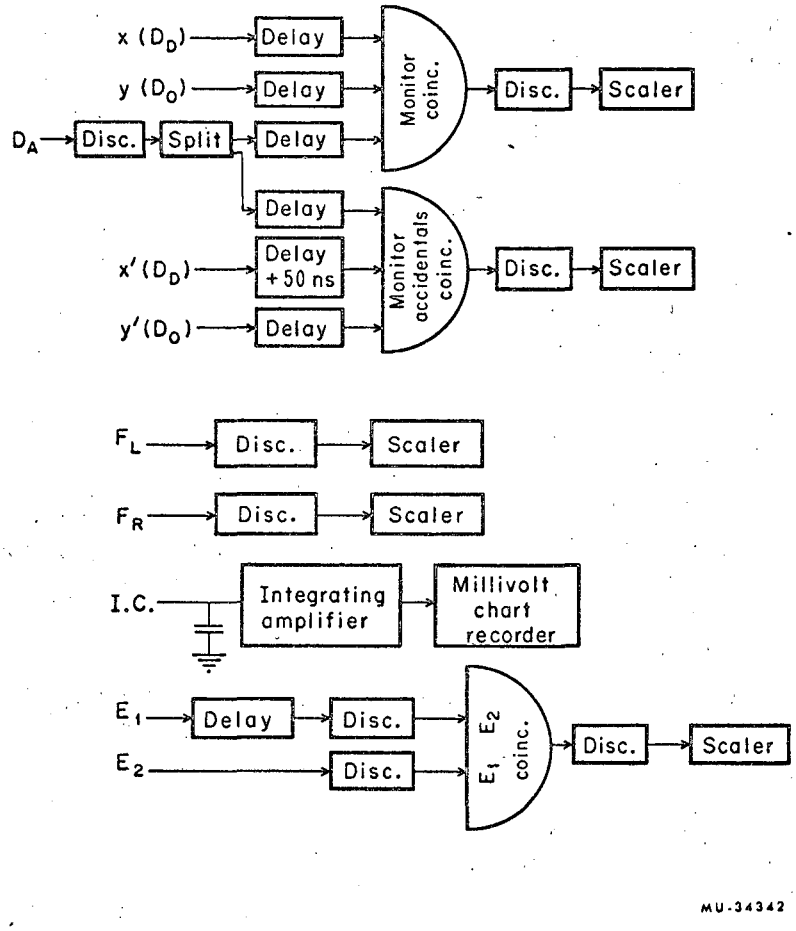

Fig. 8. Monitoring circuits.

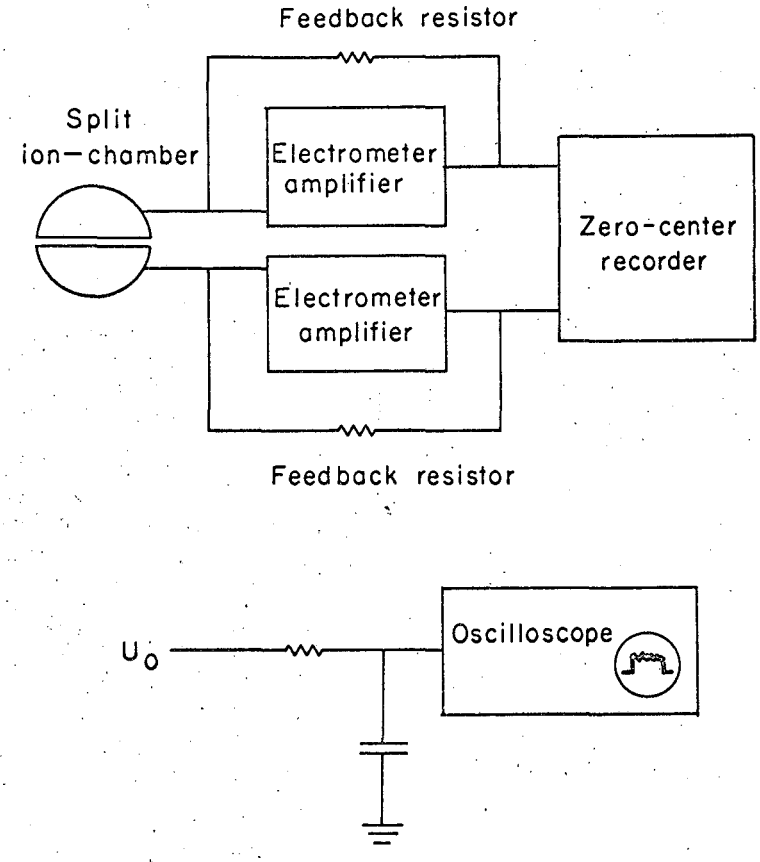

Fig. 9. Monitoring circuits.

split ion chamber.

The data are accumulated as follows. For each of the four possible combinations of beam and target polarizations (+ +, + -, - +, - -) data is taken in two or more 20-min periods gauged by 20-V sweeps of the ionization-chamber integrating-electrometer recorder using a 0.11 μf capacitor. These runs are interspersed with occasional shorter first-target-flask-empty runs to maintain a check on the purity of the beam, as well as runs with dummy target used in place of the crystals. During each 20-min run the digitized NMR signal of the polarized-target crystals is recorded on punched paper tape for future processing by computer. At the end of each data run the information stored in the 100-channel matrix of scalers is recorded on the same punched paper tape along with the contents of the various monitors. The processing of the data is described in the next chapter.

The correspondence between the counter positions and center-of-mass angles of the interactions is computed by a kinematics program which takes into account the bending of the particle trajectories in the magnetic field of the polarized-target magnet, as well as the average energy loss in the target crystals of each of the particles involved in the interaction. Given appropriate kinematic parameters the program names the counter into which the particle conjugate to a specified ray would go. In this way one can predict the location of the hydrogen events in the 100-channel matrix of ray combinations. If the reconstructed events do not coincide exactly with the observed peaks one may want to remeasure some input parameter such as beam

energy, counterposition, etc. Ultimately when agreement is reached between the computed and observed particle trajectories, the program furnishes all the center-of-mass parameters of the specified interaction off the polarized protons in the crystals.

Figure 10 is a diagram of a few trajectories computed by this ray-tracing kinematics program. They demonstrate the angular limitations of the experimental arrangement with which we are working. We see that the 100 deg c.m. ray passes through the trapezoidal section of the magnet yoke. In the case of the 40 deg c.m. interactions, the slow particles have such a range of energy loss in the target crystals that due to this effect alone the hydrogen peak broadens by the amount indicated with dotted rays. Broadening for other reasons is also enhanced, causing an unknown fraction of hydrogen peak to miss the down array or spread over what might be considered flat region. The fraction counted in the down array is then a sensitive function of such geometry changes as slight shifts in the target illumination. As a result the hydrogen-to-background ratio becomes susceptible to false asymmetries. The useful angular interval for this experiment is therefore 50 deg to 90 deg c.m. and could be increased below 50 deg by the use of thinner crystals. Alternatively one may identify the events involving the polarized protons by some means other than conjugate particle coincidences, namely fast-particle range or momentum.

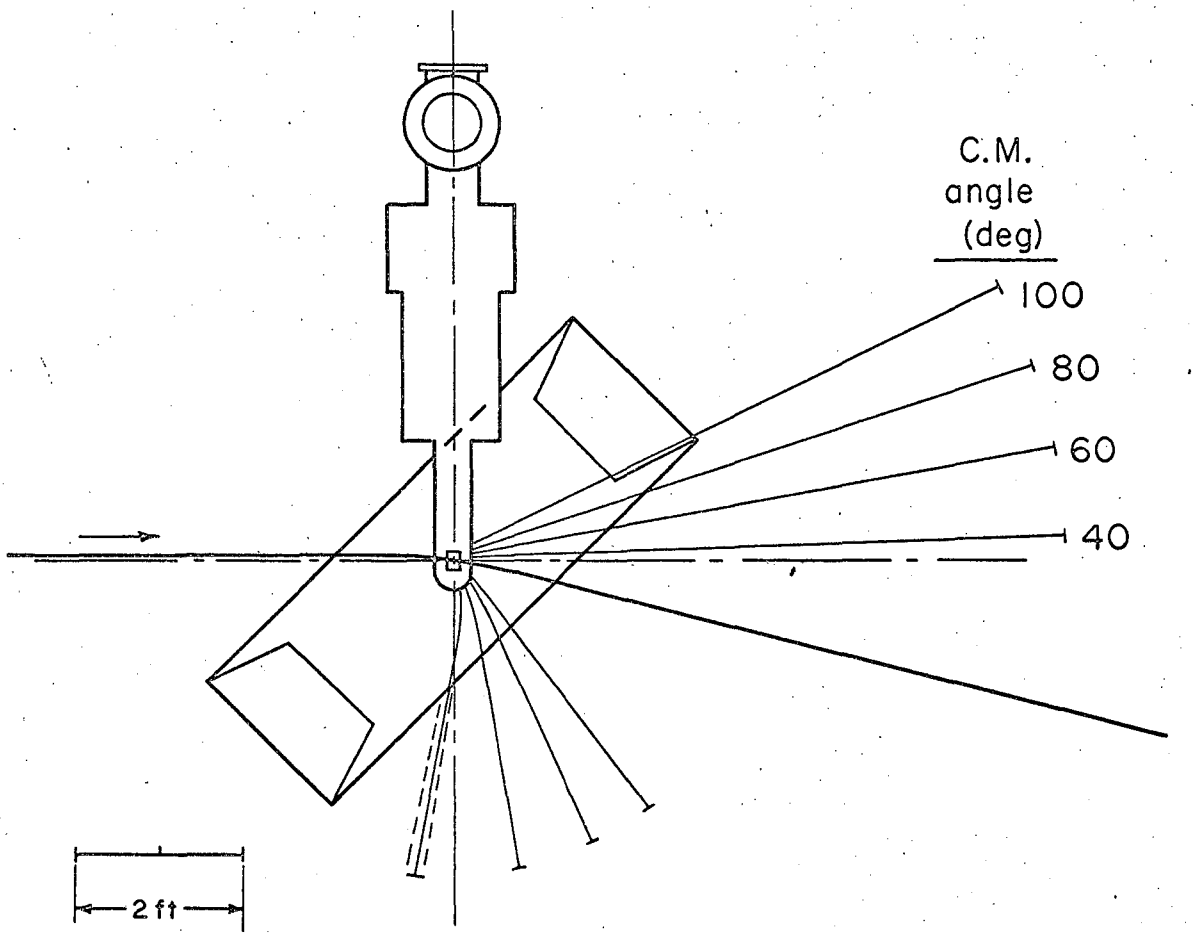

Fig. 10. Limitations in scattering angle for the apparatus used in this experiment.

IV. DATA ANALYSIS

A. Computation of the Target Polarization

Schultz[7] has shown that for moderately large enhancements the expression for the target polarization is proportional to the area under the NMR absorption curve. Since the NMR detection system actually furnishes a signal proportional to the derivative of the absorption curve, the target polarization is a number proportional to the double integral of the recorded signal, suitably corrected. Each differential curve is digitized at about 150 points, 100 of which fall into the region of integration. The computation of the double integral takes place by computer. In Fig. 11 we see some plotted computer output corresponding to a TE (thermal-equilibrium) signal and a signal of each positive and negative enhancement. On the left are the differential NMR curves as obtained during the experiment shown only in the region of integration. On the right are the corresponding first integrals for which the computer obtains the areas.

The areas thus obtained for each run furnish an enhancement factor for that run when compared to currently appropriate TE signal areas. For these TE signals one computes the polarization directly from knowledge of the magnetic field intensity and the temperature of the helium bath. This temperature is measured indirectly by measuring the vapor pressure of the helium atmosphere with an oil manometer. The overall accuracy of the manometer is believed to account for about 5% systematic uncertainty in the target polarization, while the inaccuracies in the readings account for most of the estimated 5% target-polarization random error. Betz[9b] describes improvements in

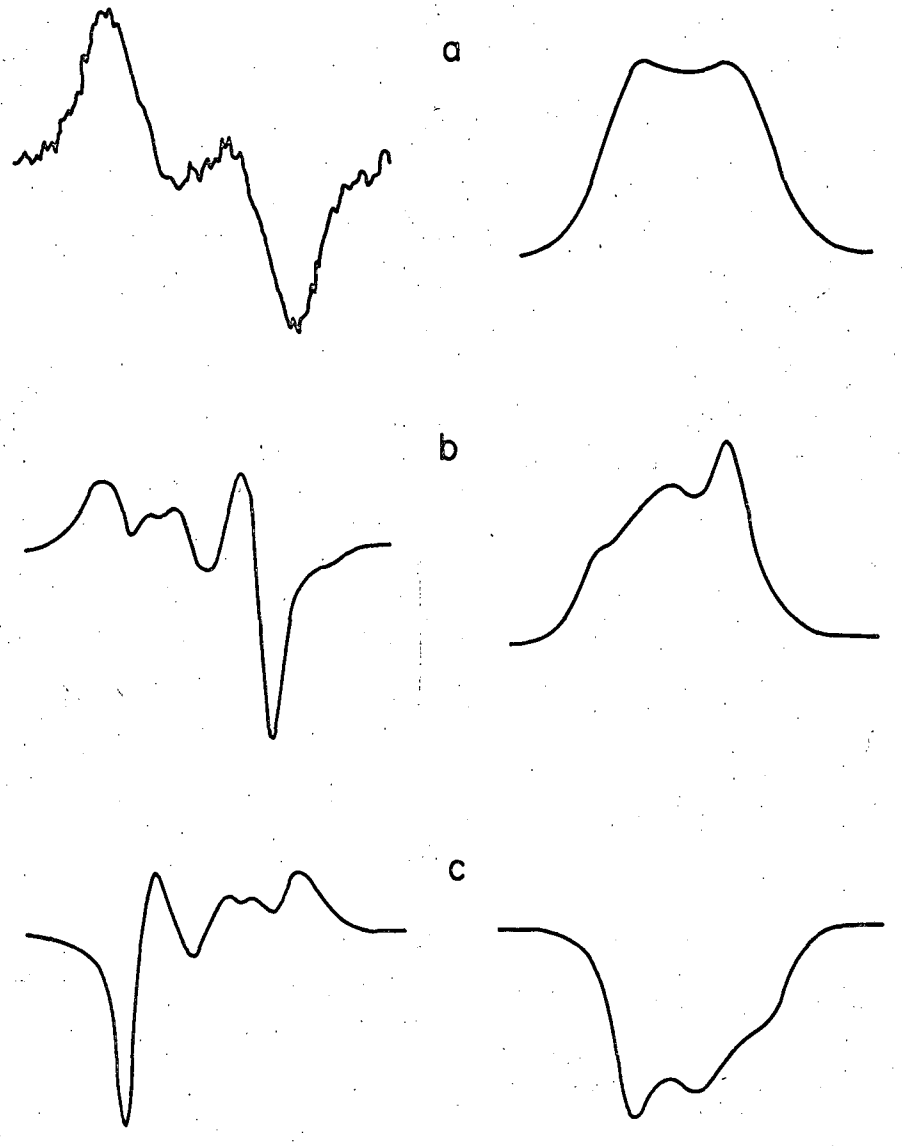

Fig. 11. Nuclear magnetic resonance signals, shown at (a) thermal equilibrium, (b) positive enhancement, and (c) negative enhancement. On the feft are the recorded differential signals, on the right the corresponding computer integrations.

target-polarization analysis since Schultz's work.

B. Computation of the Polarization Parameters

1. General Considerations

The analysis of the data will proceed as follows. Data exist for two counter positions, labeled 1 and 3, where the arrays are covering different angular regions. Position 3 includes the points more forward in the center-of-mass system. The crystal-target data for a given counter position are divided into subgroups of runs. These subgroups are likely to be mutually inconsistent because of such unavoidable geometry changes as shifts in the target location following dummy-target substitutions. The data within the subgroups are believed to be free from false asymmetries. The dummy-target data are subtracted with different normalization for each subgroup. Then the hydrogen-peak asymmetries are computed one row at a time (one row corresponding to one angle-defining counter) to give the polarization parameters for that center-of-mass angle for each subgroup of data. Finally the results from the various subgroups of one counter position are combined, suitably weighted.

Although one obtains values of $P(\theta)$, P_B, and $C_{NN}(\theta)$ for each α counter, one may further combine the results of P_B for all α counters into a grand average since P_B is not a function of second-scattering angle. The value of P_B thus obtained may then be used in a subsequent computation of C_{NN} from the same data. This procedure of feeding back the computed beam polarization is particularly useful for the counter position near 90 degree center-of-mass. There the

analyzing power of the second target gets small. This results in large statistical errors of the internally computed beam polarization, correspondingly the errors in C_{NN} derived from this internally computed P_B may be large. Here one therefore profits from using P_B derived from data from counter position 3 in the form of external input.

The polarization parameters are computed from the data using Eq. (24) for the differential cross section $I(\theta)$ when beam and target are polarized:

$$I(\theta) = I_0(\theta)\left[1 + \left(P_B+P_T\right) P(\theta) + P_B P_T C_{NN}(\theta)\right] \qquad (24)$$

We henceforth regard the symbol P_B to represent the absolute value of the beam polarization and assume that only the target polarization is fluctuating from run to run while P_B is constant. Moreover we adopt the symbol τ_i for the target polarization of the ith run (to avoid double subscripts). Then Eq. (24) may be rewritten, depending on the direction of the beam polarization,

$$I_i = I_0\left[(1 \pm P_B P) + \tau_i(P \pm P_B C_{NN})\right] \qquad (25)$$

using the upper or lower sign consistently.

We now find it convenient to introduce four new quantities A, B, C, D defined by

$$\begin{aligned} A &= I_0(1 + P_B P), & B &= I_0(P + P_B C_{NN}) \\ C &= I_0(1 - P_B P), & D &= I_0(P - P_B C_{NN}). \end{aligned} \qquad (26)$$

In terms of these quantities the polarization parameters are given by

$$I_0 = \frac{A+C}{2} \qquad P_B = \frac{A-C}{B+D}$$
$$P = \frac{B+D}{A+C} \qquad C_{NN} = \frac{1}{P_B}\,\frac{B-D}{A+C} \,. \tag{27}$$

Equations (25) then get to look like parametric equations for straight lines, e.g.

$$I_i = A + \tau_i B \,. \tag{28}$$

In reality they are equations for straight lines only if we allow i to have two values and no more, for otherwise we would be overdetermining the parameters A, B, etc. To avoid confusion we refer to the data as $I_i(\tau_i)$ and to the line, parametrized by A and B, for instance, as

$$L_i(\tau_i) = A + \tau_i B \,.$$

We shall therefore compute C_{NN} and the other parameters by finding the straight line for each of the two beam polarizations that best fits the data by the well-known technique of minimizing the sum of the squares of the deviations of the actual data points from the line.[11]

2. Straight-Line Fitting

We define the deviation of the ith data point from the line parametrized by A and B by

$$I_i - L_i(A,B)$$

Minimizing the sum of the squares of these deviations means solving a pair of equations for each pair of parameters (we treat only one pair, A and B), namely

$$\frac{\partial}{\partial A} \sum \left[I_i - L_i(A,B) \right]^2 = 0$$

$$\frac{\partial}{\partial B} \sum \left[I_i - L_i(A,B) \right]^2 = 0 .$$

If the various runs are not for the same number of monitors m_i, we account for the different lengths by normalizing the data $I_i \to \frac{I_i}{m_i}$ and furthermore weighting the squared deviations by the monitors. This latter procedure is equivalent to considering a run of twice ordinary length equivalent to two runs of ordinary length, yielding two data points, each contributing one term to the sum of squared deviations. We finally write

$$\frac{\partial}{\partial A} \sum m_i \left[\frac{I_i}{m_i} - L_i(A,B) \right]^2 = 0$$

$$\frac{\partial}{\partial B} \sum m_i \left[\frac{I_i}{m_i} - L_i(A,B) \right]^2 = 0 . \qquad (30)$$

It is easy to solve these equations. One obtains

$$A = \bar{I} - B\bar{\tau} \qquad B = \frac{\overline{I\tau} - \bar{I}\bar{\tau}}{\overline{\tau^2} - \bar{\tau}^2} \qquad (31)$$

where we have defined

$$\bar{I} = \frac{\sum I_i}{\sum m_i} \qquad \bar{\tau} = \frac{\sum m_i \tau_i}{\sum m_i}$$

$$\overline{I\tau} = \frac{\sum I_i}{\sum m_i} \qquad \overline{\tau^2} = \frac{\sum m_i \tau_i^2}{\sum m_i} . \qquad (32)$$

3. Dummy-Target Subtractions

Equations (31) would lead to the elastic proton-proton polarization parameters only if I_i were events involving pure second-target polarized protons. For the purpose of data handling it is convenient to think of the I_i as the hydrogen-peak-region crystal-target data of a given row of the 10 × 10 data matrix including events involving the unpolarized background. We must then describe how to subtract the background by means of the dummy-target data.

For a given counter position we define those elements of the 100-channel crystal-target data matrix that contain any portion of the hydrogen peak as peak region, and all the rest as flat region. This designation is maintained for the dummy-target data. The sum of all the elements in the flat region of the ith crystal-data run we call F_{Ci}, while the corresponding dummy-target quantity summed over all runs is F_D. For the row under analysis we call the sum of the crystal-data peak-region elements I_i and the corresponding dummy-target quantity summed over all runs J.

In terms of these quantities, pure hydrogen (polarized target proton) events are then given by

$$I_i - F_{Ci} \frac{J}{F_D} .$$

We may retain the definitions stated in expression (32) and modify only the equation for A in Eqs. (31)

Table V. Results for $P(\theta)$ and $C_{NN}(\theta)$ of proton-proton elastic scattering at 680 MeV.; t is the invariant four-momentum transfer squared; in addition to the random errors quoted, there are systematic fractional errors of 5% on P and 10% on C_{NN}.

θ_{cm} (deg)	$-t$ 10^5 (MeV/c)^2	$P(\theta)$	$C_{NN}(\theta)$
51.2	2.38	0.472 ± .053	0.449 ± .122
54.3	2.66	0.564 ± .041	0.570 ± .097
57.4	2.94	0.528 ± .039	0.543 ± .092
60.5	3.24	0.494 ± .041	0.545 ± .097
63.7	3.54	0.386 ± .042	0.708 ± .100
66.7	3.86	0.375 ± .043	0.665 ± .104
70.8	4.27	0.384 ± .032	0.574 ± .079
73.7	4.58	0.317 ± .027	0.603 ± .069
76.7	4.90	0.252 ± .028	0.752 ± .075
79.6	5.22	0.189 ± .029	0.806 ± .078
82.6	5.55	0.175 ± .030	0.731 ± .079
85.6	5.88	0.129 ± .039	0.909 ± .101
88.7	6.22	0.004 ± .053	0.835 ± .128

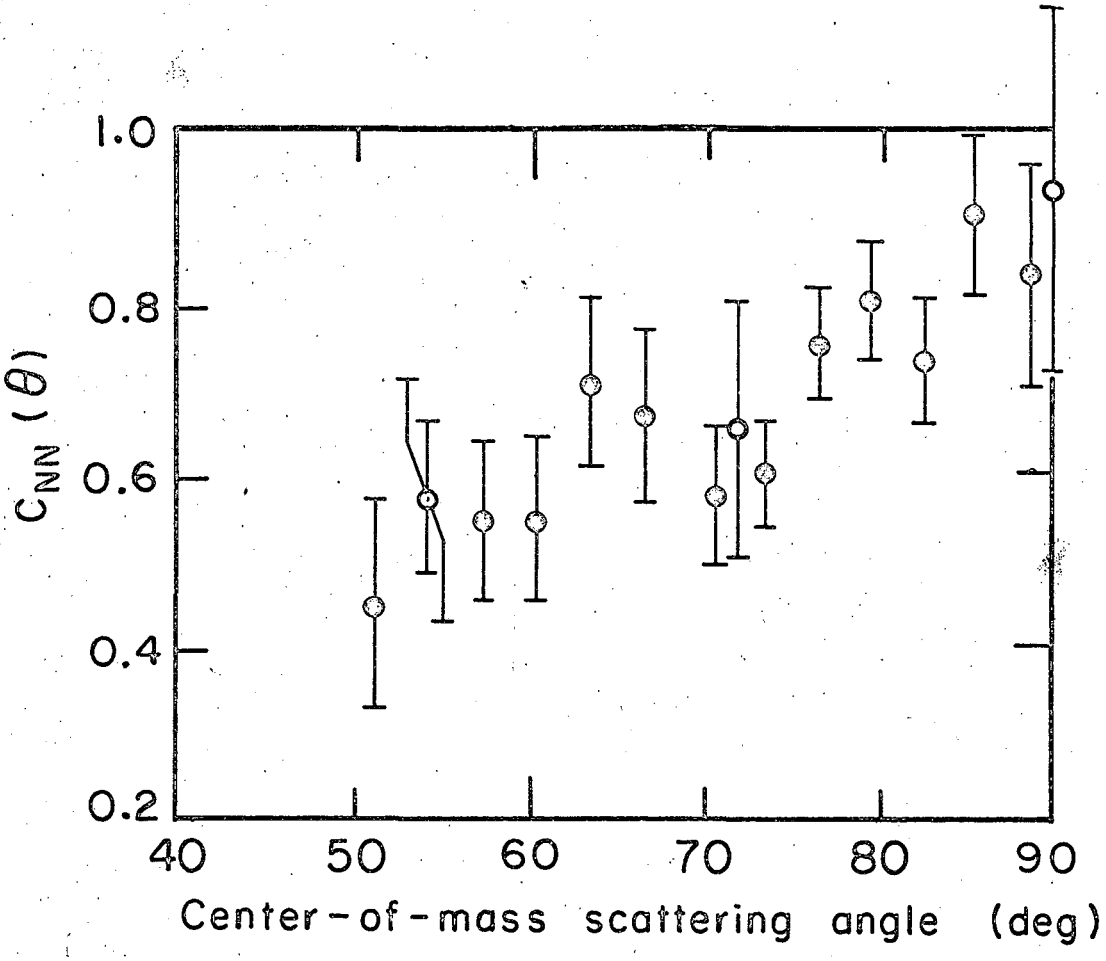

MU-35185

Fig. 12. Results of this experiment: $C_{NN}(\theta)$ in elastic proton-proton scattering at 680 MeV. (The open circles are the results of Ref. (5f) at 640 MeV.) A 10% fractional error due to a systematic uncertainty in the target polarization should be added in quadrature to the errors shown.

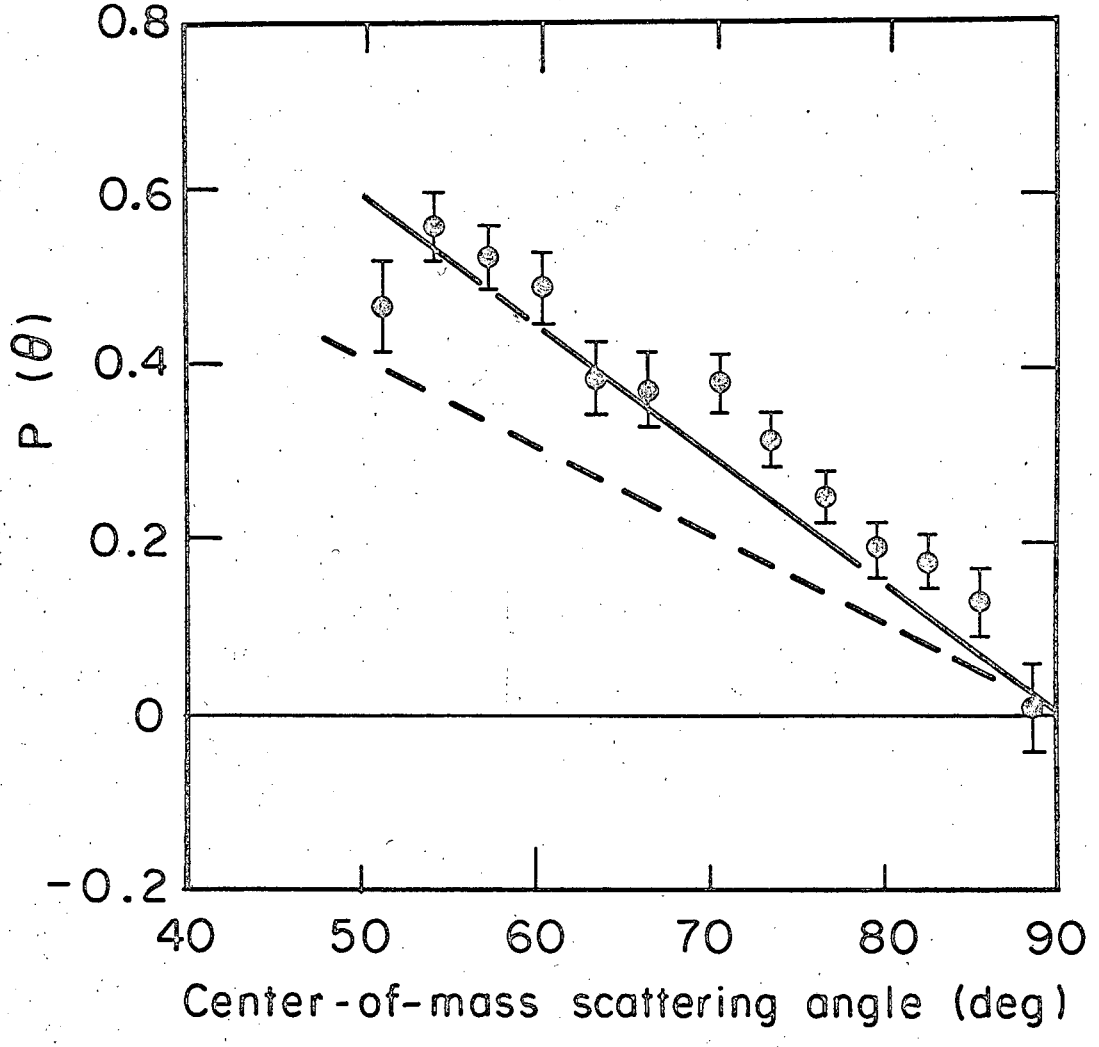

MU-35186

Fig. 13. Results of this experiment: $P(\theta)$ in elastic proton-proton scattering at 680 MeV. A 5% fractional error due to a systematic uncertainty in the target polarization should be added in quadrature to the errors shown. The solid straight line represents a good fit to the data of Betz[9b] at this energy while the dashed line corresponds to data of Ref. (12) at 660 MeV.

$$A = \bar{I} - \overline{F_C}\,\frac{J}{F_D} - B\bar{\tau}$$

$$B = \frac{\overline{I\tau} - \bar{I}\bar{\tau}}{\overline{\tau^2} - \bar{\tau}^2} \,. \qquad (33)$$

Here we have defined

$$\overline{F_C} = \frac{\sum F_{Ci}}{\sum m_i} \,. \qquad (34)$$

It is easy to verify that the background does not appear explicitly in the expression for B .

If Eqs. (33) and the corresponding equations for C and D are used to compute the results one obtains the values published in Table V and Figs. 12 and 13. Among the results is also the quantity P_B which has the value

$$P_B = 0.44 \pm 0.02 \,.$$

4. Classification of Errors

The independent quantities that lead to the polarization parameters are readily identified to be I_i , F_C , F_D, J, , τ_i , and, if external, P_B. They all contribute to errors in the results. We consider the monitors m_i known with negligible error. The expressions for the errors are developed in Appendix C.

When it comes to combining results, as for instance averaging

$P(\theta)$ for one α counter over a number of subgroups, we need to use weight factors composed of errors that are uncorrelated within each subgroup. That requirement would include errors due to only I_i, F_C, and τ_i (random) in the weighting of the individual $P(\theta)$ above. It is therefore important to classify the sources of error according to the extent of their correlation in a given result, as shown in Table VI. The errors that are uncorrelated for all the quantities to be averaged and therefore suitable for weighting, get diminished in the combining process, while those correlated get averaged.

We explain the procedure in some detail with an example. Let us assume we have computed $P(\theta)$, P_B, and $C_{NN}(\theta)$ (internal P_B) using the peak-region data (I_i) of counter α_1 of a certain subgroup of mutually compatible crystal-target runs, their target polarization (τ_i), the flat region count (F_C) for all the runs in the subgroup, the peak-region data of this counter summed over all the dummy-target runs available at this counter position (J), and the total dummy-target-flat-region count of the same runs (F_D). All of the quantities computed have errors due to the various sources enumerated. We compute these errors and combine those belonging to the same class of errors in quadrature. If we go through a similar computation for the same counter using a different subgroup of crystal-target data runs, we arrive at different results of $P(\theta)$, P_B and $C_{NN}(\theta)$ and their errors in the four different classes.

To average the results of these two computations from different

Table VI. Classification of the errors according to correlation

Class of error	Source of error	Error correlated for each α counter	Error correlated for each data subgroup
1	I_i	no	no
2	F_C, τ_i(random)	yes	no
3	J	no	yes
4	F_D, τ_i(syst.), P_B(if ext.)	yes	yes

subgroups of runs we need to consult Table VI for the correct weight factors. We see that the errors in classes 1 and 2 are uncorrelated for each subgroup. We therefore proceed to combine the errors in classes 1 and 2 in quadrature for each quantity to be averaged and use as weight factor the inverse squares of the combined error, thus

$$\bar{P} = \frac{\sum \omega_i P_i}{\sum \omega_i} \tag{35}$$

Here $\bar{P}$ is the result of averaging the P_i, the computed value of $P(\theta)$ for the ith subgroup. The weight factors ω_i are defined in terms of the errors in classes 1 and 2, δ_1 and δ_2, by

$$\omega_i = \frac{1}{(\delta_1^2+\delta_2^2)_i}$$

The errors in $\bar{P}$ of these two classes reduce according to the rule

$$\frac{1}{(\delta_{1,2})^2} = \sum \frac{1}{(\delta_{1,2})_i^2}$$

while those of classes 3 and 4 average in the manner of Eq. (35). Ultimately we may combine the errors thus obtained in classes 1 and 3 in quadrature into the final errors in class 3 and those of classes 2 and 4 into final class 4 errors.

5. Sample Calculation

This calculation using the data of a small number of runs is intended to convey a feeling for the rate of data accumulation when one uses a polarized target. We have chosen a set of runs at random. To simplify the computation we shall substitute uniform values for the target polarization and the monitors. Otherwise the calculation is standard. We shall compute the asymmetries for only one angle-defining α counter, although at this counter position we have analyzable hydrogen peaks for six α counters. We use the full flat region to normalize the dummy-target data.

The crystal-target data were accumulated in a single period of 16 hours, including one hour at the beginning and at the end for thermal-equilibrium NMR signals. The data runs cycle through the four combinations of the beam and target polarizations twice, with two runs taken at each combination separated by a first-target-flask-empty run of half normal duration. We do not use the flask-empty runs in the analysis. The data therefore consist of a total of 16 runs (actually 17, since they include two runs of half normal duration) labeled intermittently between Nos. 500 and 526.

The dummy-target data used in this sample calculation consist of three runs at each beam polarization. They are labeled Nos. 629 to 634 and were taken during a period of about three hours.

We assume uniform target polarization of ± 0.50, beam polarization of ± 0.50, and monitors m_i of 1.00 (or 0.50 for the two short runs). Typical STOT count was 3000, of which about 1 percent was rejected

due to multiple coincidences in one of the counter arrays. The monitor circuits had about 5 percent accidental rate. Typical I_i is 100 to 300, depending on the initial-state polarization.

The quantities composing A, B, C, and D are shown in Table VII. They give

$$A = 186.4 \qquad B = 76.0$$

$$C = 120.0 \qquad D = 18.5.$$

Using Eqs. (27) we finally have

$$P_B = \frac{A - C}{B + D} = 0.703$$

$$P(\theta) = \frac{B + D}{A + C} = 0.308$$

$$C_{NN}(\theta) = \frac{1}{P_B} \frac{B - D}{A + C} = \frac{B^2 - D^2}{A^2 - C^2} = 0.267.$$

If we assume $P_B = 0.50$, externally given, we get

$$C_{NN}(\theta) = 0.375$$

We calculate the errors for this external-P_B C_{NN} using the expressions of Appendix C. If we assume 5 percent random error in $(\Delta\tau/\tau)_2$ and an error in the beam polarization of $(\Delta P_B/P_B)_4 = 0.025$, we find the errors listed in Table VIII. In the table they are compared to the errors obtained with all the correct experimental quantities, i.e. the real monitors and target polarizations, for both external and internal beam polarizations.

Table VII. Intermediate steps in the sample calculation.

P_B	Positive	Positive	Negative	Negative
Target	Crystal	Dummy	Crystal	Dummy
Σm_i	8.0	3.0	8.0	3.0
ΣF_{Ci}, ΣF_{Di}	7286	2740	7119	2500
$\overline{F}_C$, $\overline{F}_D$	910.75	913.33	889.9	833.33
ΣI_i, ΣJ_i	2148	247	1564	212
$\overline{I}$, $\overline{J}$	268.5	82.33	195.5	70.67
$\Sigma I_i \tau_i$	152.0	-	37.0	-
$\overline{I\tau}$	19.0	-	4.625	-
$\overline{\tau^2}$	0.25	-	0.25	-

Table VIII. Comparison of the errors in C_{NN} for sample-calculation and real-data values of the target polarization.

Error class	Sample calculation	Real data internal P_B	Real data external P_B
1	± .099	± .153	± .135
2	± .010	± .019	± .014
3	± .005	± .000	± .001
4	± .019	± .002	± .027
C_{NN}[a]	.375	.440	.504

[a] These are the values of the parameters in the respective columns and not corresponding errors.

The differences in the errors arise primarily from finite $\bar{\tau}$ of the real data, that is, from the fact that the average positive polarization was slightly different in magnitude than the average negative polarization. We note that the main contribution to the random error is the statistical fluctuation of the hydrogen-peak data.

C. Discussion of Results

The results for $P(\theta)$ and $C_{NN}(\theta)$ are listed in Table V together with their random errors. They are also shown plotted in Figs. 12 and 13. We ascribe a systematic fractional error of 5% to the values of the enhanced target polarization obtained from the NMR signals and the computed TE polarization. Accordingly there is fractional systematic uncertainty of 5% in all the values of $P(\theta)$ and of 10% in $C_{NN}(\theta)$.

It should be noted how remarkable the agreement is between our results for C_{NN} and those of Ref. (5f). On the other hand while our results for P agree well with Betz[9b] they deviate considerably from those of Ref. (12). The results of Refs. (5f) and (12) were recently used in searches for proton-proton phase shifts at 660 MeV.[13]

Stapp has pointed out that at 90 deg center-of-mass the value of C_{NN} contains information about the singlet-triplet content of the interaction.[3] A value of +1 represents pure triplet scattering while -1 would be pure singlet. Evidently at this energy the triplet amplitudes predominate.

It is clear that the polarized target offers an advantageous scheme for measuring the polarization correlation, C_{NN} . Good

accuracy of measurement can be combined with the feature of counting at several scattering angles at the same time. A comparison of Tables II and V brings out the value of using a polarized target.

Given results for a great variety of experiments at one energy, one would expect to determine fully all the scattering amplitudes at that energy. At present this is not practicable because many of the necessary experiments have not yet been performed at our energy.

It is possible to estimate how much information is needed to determine fully the scattering amplitude at one energy. At lower energy (310 MeV), where the proton-proton scattering could be assumed to be purely elastic, Stapp, Ypsilantis, and Metropolis were able to reduce the ambiguities to the point that only a few possible sets of phase shifts were consistent with the experimental data.[14] They had available to them measurements of the differential cross section I_o, the polarization P, the depolarization D, and the rotation parameters A and R (D, A, and R over about half the full range of scattering angles). We therefore estimate that at our higher energy, at which much inelastic scattering occurs, one would probably need I_o, P, D, R, A, C_{NN}, and perhaps C_{KP} measured over the full range of scattering angles to reach the point of a completely unambiguous set of phase shifts (and hence scattering amplitudes). This set happens to constitute one of the complete sets suggested by Schumacher and Bethe.[4] Consequently it seems premature to attempt the proposed phase shift analysis at the present, when less than half the necessary experiments have been performed.

It is sometimes possible to carry out a complete analysis with fewer kinds of experiments performed at one energy if results at many energies are combined with the requirement that the phase shifts vary slowly as functions of energy. Such a procedure has been used by Breit et al.[15] and Stapp et al.[16].

It is in any case beyond the scope of the present work to attempt this analysis. Perhaps as more data are available, some of them from further experiments using the polarized target, we may be encouraged to attempt the search for the unique scattering amplitudes at this energy.

V. CONCLUSION

We have presented results of a proton-proton scattering experiment in which both initial state particles were polarized. In quality and amount the results demonstrate that the polarized target is an important tool in the measurement of the parameter C_{NN}. Ultimately the results will be valuable in the construction of the scattering matrix.

ACKNOWLEDGMENTS

My thanks go to Professor Owen Chamberlain for his guidance during my graduate study. It was he who proposed this experiment. His careful attention to detail, patience, and integrity have been inspiring.

In the sense in which this experiment was conducted jointly with others the name that naturally heads the list of collaborators is that of my good friend Fred Betz. To him and to Professors Claude Schultz and Gilbert Shapiro, as well as Dr. Leland Holloway I express my appreciation for hard work at odd hours and for good advice in discussions. To my fellow graduate students John F. Arens and Michel Hansroul I owe thanks for the same reasons in slightly different proportions. Among others I also thank my friend Bill Troka for his valuable help in time of need.

Professor Herbert Steiner and Dr. Ludwig Van Rossum were among those who originally designed much of the equipment that was later used in this experiment.

Among the many names that come to mind in connection with the smooth operation of the experiment are those of Jimmy Vale and his cyclotron staff, notably Bob Walton and Lou Sylvia, Fred Kirsten, Quentin Kerns and Lee Wagner and their electronics design and maintenance groups, Ed McLaughlin and his very fine cryogenics engineers and technicians, and Jim Baker and the computer programmers and operators.

All of the typing under often trying conditions was done by our secretary. My sincere thanks, Rosemary.

I would also like to express my gratitude to Professors Zemach

and Brewer for reading this thesis on short notice.

If it is proper to dedicate a thesis to someone, I dedicate mine gratefully to my valiant mate. May your future be brighter, Sylvia. I also dedicate this thesis to the memory of my Mother. She would have been very happy.

The U. S. Atomic Energy Commission has lent some indispensable financial support during most of my graduate study. In fact all of this work was done under the auspices of this agency.

APPENDICES

A. Composite-Spin-Space Components

We show here how one relates the components of individual particle spinors to the components of the combined spin space spinors for the special case of two particles of spin 1/2.

Let the individual particle spinors be r and s each of two components. Let the combined spinor be the four component object X. If A is an operator in the space of r, B in the space of s, the we define C as the corresponding operator in the composite spin space operating on X such that

$$CX = ArBs$$

The corresponding relation between the component is

$$C_{ij}X_j = A_{k\ell}r_\ell B_{mn}s_n = A_{k\ell}B_{mn}r_\ell s_n \ . \qquad \text{(A-1)}$$

For the special case where A, B, and C are the identity operators, this relation reduces to

$$X_j = r_\ell s_n \ .$$

There j ranges from 1 to 4 while ℓ and n are 1 or 2. The only two ways in which the indices ℓ and n can be combined to give the four different j uniquely are

$$j = 2(\ell-1) + n \quad \text{and} \quad j = 2(n-1) + \ell \ .$$

Any other combination fails to define one or more of the subscripts j in terms of ℓ and n, i.e. one or more of the components of X in terms of the components of r and s. The two different relations are equivalent in the sense that they each give a unique set of well defined components different only by an interchange of second and third

components. However, one has to agree to use only one of them consistently. We shall use the former. Equation (A-1) then becomes

$$A_{k\ell}B_{mn}r_{\ell}s_{n} = C_{2(k-1)+m,\,2(\ell-1)+n}\,X_{2(\ell-1)+n} \,.$$

B. Proof of Equation (23)

We want to verify Eq. (23) of Chapter II

$$\mathrm{Tr}(\sigma_{1N}\sigma_{2N})M\,M^{\dagger} = \mathrm{Tr}\,M(\sigma_{1N}\sigma_{2N})M^{\dagger} \,. \tag{B-1}$$

We use the commutation relations of the Pauli spin matrices

$$\sigma_j\sigma_k = \delta_{jk} + i\,\epsilon_{jk\ell}\sigma_{\ell} \tag{B-2}$$

as well as the identities

$$\sigma_j^{\dagger} = \sigma_j$$

$$\mathrm{Tr}\,\sigma_j = 0$$

where j, k, and ℓ run over x, y, and z and

$$\delta_{jk} = \begin{cases} 1 \text{ for } j = k \\ 0 \text{ for } j \neq k \end{cases}$$

$$\epsilon_{jk\ell} = \begin{cases} 1 \text{ for } jk\ell = xyz \text{ or cyclic permutation thereof} \\ -1 \text{ for } jk\ell = xzy \text{ or cyclic permutation thereof} \\ 0 \text{ for any two indices the same.} \end{cases}$$

We also note that operators belonging to different spin spaces commute (i.e., $\sigma_{j1}\sigma_{k2} = \sigma_{k2}\sigma_{j1}$).

Using (B-2) we can also show that

$$\sigma_{\alpha}\sigma_{\beta} = \delta_{\alpha\beta} + i\,\epsilon_{\alpha\beta\gamma}\sigma_{\gamma}$$

where this time α, β, and γ are $\hat{N}$, $\hat{K}$ and $\hat{P}$.

To see this illustrated we evaluate

$$\begin{aligned}\sigma_{1N}\sigma_{1K} &= (\sigma_{x1}N_x + \sigma_{y1}N_y + \ldots)\cdot(\sigma_{x1}K_x + \ldots)\\ &= N_xK_x\sigma_{x1}\sigma_{x1} + N_xK_y\sigma_{x1}\sigma_{y1} + \ldots\\ &= N_xK_x + N_xK_y(i\,\sigma_{z1}) + \ldots\\ &= \hat{N}\cdot\hat{K} + i\,\vec{\sigma}_1\cdot(\hat{N}\times\hat{K})\\ &= i\,\vec{\sigma}_1\cdot\hat{P} = i\,\sigma_{1P}\,.\end{aligned}$$

since $\hat{N}$, $\hat{K}$, and $\hat{P}$ make up a right-handed coordinate system in that order.

For $M(\theta)$ we use Wolfenstein's form

$$M(\theta) = B + C(\sigma_{1N}+\sigma_{2N}) + N\sigma_{1N}\sigma_{2N} + \tfrac{1}{2}G(\sigma_{1P}\sigma_{2P}+\sigma_{1K}\sigma_{2K}) - \tfrac{1}{2}H(\sigma_{1P}\sigma_{2P}-\sigma_{1K}\sigma_{2K}).$$

Therefore we have for $M^\dagger$

$$[M(\theta)]^\dagger = B^* + C^*(\sigma_{1N}+\sigma_{2N}) + N^*\sigma_{1N}\sigma_{2N} + \tfrac{1}{2}G^*(\sigma_{1P}\sigma_{2P}+\sigma_{1K}\sigma_{2K}) - \tfrac{1}{2}H^*(\sigma_{1P}\sigma_{2P}-\sigma_{1K}\sigma_{2K}).$$

We now compute the required product matrices.

$$\begin{aligned}MM^\dagger = {} & BB^* + BC^*(\sigma_{1N}+\sigma_{2N}) + BN^*\sigma_{1N}\sigma_{2N} + \tfrac{1}{2}BG^*(\sigma_{1P}\sigma_{2P}+\sigma_{1K}\sigma_{2K})\\ & - \tfrac{1}{2}BH^*(\sigma_{1P}\sigma_{2P}-\sigma_{1K}\sigma_{2K}) + CB^*(\sigma_{1N}+\sigma_{2N}) + 2CC^*(1+\sigma_{1N}\sigma_{2N})\\ & + CN^*(\sigma_{1N}+\sigma_{2N}) + iCH^*(\sigma_{1P}\sigma_{2K}+\sigma_{1K}\sigma_{2P}) + NB^*\sigma_{1N}\sigma_{2N}\\ & + NC^*(\sigma_{1N}+\sigma_{2N}) + NN^* - \tfrac{1}{2}NG^*(\sigma_{1P}\sigma_{2P}+\sigma_{1K}\sigma_{2K})\\ & - \tfrac{1}{2}NH^*(\sigma_{1P}\sigma_{2P}-\sigma_{1K}\sigma_{2K}) + \tfrac{1}{2}GB^*(\sigma_{1P}\sigma_{2P}+\sigma_{1K}\sigma_{2K})\\ & - \tfrac{1}{2}GN^*(\sigma_{1P}\sigma_{2P}+\sigma_{1K}\sigma_{2K}) + \tfrac{1}{2}GG^*(1-\sigma_{1N}\sigma_{2N})\\ & - \tfrac{1}{2}HB^*(\sigma_{1P}\sigma_{2P}-\sigma_{1K}\sigma_{2K}) - iHC^*(\sigma_{1P}\sigma_{2K}+\sigma_{1K}\sigma_{2P})\\ & - \tfrac{1}{2}HN^*(\sigma_{1P}\sigma_{2P}-\sigma_{1K}\sigma_{2K}) + \tfrac{1}{2}HH^*(1+\sigma_{1N}\sigma_{2N})\end{aligned}$$

$$\sigma_{1N}\sigma_{2N} MM^\dagger = BB^*\sigma_{1N}\sigma_{2N} + BC^*(\sigma_{1N}+\sigma_{2N}) + BN^*$$
$$-\tfrac{1}{2}BG^*(\sigma_{1P}\sigma_{2P}+\sigma_{1K}\sigma_{2K}) - \tfrac{1}{2}BH^*(\sigma_{1P}\sigma_{2P}-\sigma_{1K}\sigma_{2K})$$
$$+CB^*(\sigma_{1N}+\sigma_{2N}) + 2CC^*(1+\sigma_{1N}\sigma_{2N})$$
$$+CN^*(\sigma_{1N}+\sigma_{2N}) + iCH^*(\sigma_{1P}\sigma_{2K}+\sigma_{1K}\sigma_{2P}) + NB^*$$
$$+NC^*(\sigma_{1N}+\sigma_{2N}) + NN^*\sigma_{1N}\sigma_{2N} + \tfrac{1}{2}NG^*(\sigma_{1P}\sigma_{2P}+\sigma_{1K}\sigma_{2K})$$
$$-\tfrac{i}{2}NH^*(\sigma_{1P}\sigma_{2P}-\sigma_{1K}\sigma_{2K}) - \tfrac{1}{2}GB^*(\sigma_{1P}\sigma_{2P}+\sigma_{1K}\sigma_{2K})$$
$$+\tfrac{1}{2}GN^*(\sigma_{1P}\sigma_{2P}+\sigma_{1K}\sigma_{2K}) - \tfrac{1}{2}GG^*(1-\sigma_{1N}\sigma_{2N})$$
$$-\tfrac{1}{2}HB^*(\sigma_{1P}\sigma_{2P}-\sigma_{1K}\sigma_{2K}) + iHC^*(\sigma_{1P}\sigma_{2K}+\sigma_{1K}\sigma_{2P})$$
$$-\tfrac{1}{2}HN^*(\sigma_{1P}\sigma_{2P}-\sigma_{1K}\sigma_{2K}) + \tfrac{1}{2}HH^*(1+\sigma_{1N}\sigma_{2N})$$

$$\sigma_{1N}\sigma_{2N} M^\dagger = B^*\sigma_{1N}\sigma_{2N} + C^*(\sigma_{1N}+\sigma_{2N}) + N^* - G^*\tfrac{1}{2}(\sigma_{1P}\sigma_{2P}+\sigma_{1K}\sigma_{2K})$$
$$+\tfrac{1}{2}H^*(\sigma_{1K}\sigma_{2K}-\sigma_{1P}\sigma_{2P})$$

$$M\sigma_{1N}\sigma_{2N}M^\dagger = BB^*\sigma_{1N}\sigma_{2N} + BC^*(\sigma_{1N}+\sigma_{2N}) + BN^* - \tfrac{1}{2}BG^*(\sigma_{1P}\sigma_{2P}+\sigma_{1K}\sigma_{2K})$$
$$-\tfrac{1}{2}BH^*(\sigma_{1P}\sigma_{2P}-\sigma_{1K}\sigma_{2K}) + CB^*(\sigma_{1N}+\sigma_{2N}) + 2CC^*(1+\sigma_{1N}\sigma_{2N})$$
$$+CN^*(\sigma_{1N}+\sigma_{2N}) + iCH^*(\sigma_{1P}\sigma_{2K}+\sigma_{1K}\sigma_{2P}) + NB^*$$
$$+NC^*(\sigma_{1N}+\sigma_{2N}) + NN^*\sigma_{1N}\sigma_{2N} + \tfrac{1}{2}NG^*(\sigma_{1P}\sigma_{2P}+\sigma_{1K}\sigma_{2K})$$
$$-\tfrac{1}{2}NH^*(\sigma_{1P}\sigma_{2P}-\sigma_{1K}\sigma_{2K}) - \tfrac{1}{2}GB^*(\sigma_{1P}\sigma_{2P}+\sigma_{1K}\sigma_{2K})$$
$$+\tfrac{1}{2}GN^*(\sigma_{1P}\sigma_{2P}+\sigma_{1K}\sigma_{2K}) - \tfrac{1}{2}GG^*(1-\sigma_{1N}\sigma_{2N})$$
$$-\tfrac{1}{2}HB^*(\sigma_{1P}\sigma_{2P}-\sigma_{1K}\sigma_{2K}) - iHC^*(\sigma_{1P}\sigma_{2K}+\sigma_{1K}\sigma_{2P})$$
$$-\tfrac{1}{2}HN^*(\sigma_{1P}\sigma_{2P}-\sigma_{1K}\sigma_{2K}) + \tfrac{1}{2}HH^*(1+\sigma_{1N}\sigma_{2N})$$

As a result we find that indeed

$$\begin{aligned} \mathrm{Tr}\ \sigma_{1N}\sigma_{2N}\, M\, M^{\dagger} &= \mathrm{Tr}\ M\, \sigma_{1N}\sigma_{2N}\, M^{\dagger} \\ &= 2\ \mathrm{Re}(BN^{*}) - 2|C|^{2} - \tfrac{1}{2}\left[\,|G|^{2} - |H|^{2}\,\right] \end{aligned} \tag{B-3}$$

as was to be shown.

We briefly mention how the time-reversal-invariance violating amplitudes enter into C_{NN}. In terms of the time-reversal-invariant scattering matrix M the time-reversal-invariance violating scattering matrix M' is given by

$$M' = M + J\ \sigma_{1P}\sigma_{2K} + L\ \sigma_{1K}\sigma_{2P}\ .$$

We find by means demonstrated above that

$$\mathrm{Tr}\ M'\ \sigma_{1N}\sigma_{2N}(M')^{\dagger} = \mathrm{Tr}\ M\ \sigma_{1N}\sigma_{2N}\, M^{\dagger} + 2\mathrm{Re}(JL^{*})\ ,$$

and

$$\mathrm{Tr}\ \sigma_{1N}\sigma_{2N}\, M'(M')^{\dagger} = \mathrm{Tr}\ \sigma_{1N}\sigma_{2N}\, M\, M^{\dagger} + 2\mathrm{Re}(JL^{*})\ ,$$

whence because of Eq. (B-3)

$$\mathrm{Tr}\ \sigma_{1N}\sigma_{2N}\, M'(M')^{\dagger} = \mathrm{Tr}\ M'\ \sigma_{1N}\sigma_{2N}(M')^{\dagger}\ .$$

This means that the value $C_{NN}(\theta)$ is the same whether initial or final state polarizations are determined, however large the time-reversal-invariance violating amplitudes may be.

Therefore the time reversal content of our experiment is limited to the time reversal content of our measurement of $P(\theta)$.

C. Error Expressions

We use the well known formula applicable in the case of uncorrelated errors. Let x_i be i independent numbers, with errors Δx_i, that combine into a resule X. Then ΔX, the error in X due to the errors Δx_i, is given by

$$(\Delta X)^2 = \sum \left(\frac{\partial X}{\partial x_i}\right)^2 (\Delta x_i)^2 \qquad \text{(C-1)}$$

We derive only the errors of C_{NN} for the case of external beam polarization and quote all the other errors without derivation. We use the quantities given in expressions (27), (32), (33), and (34) of Chapter IV and evaluate the necessary partial derivatives.

$$\left.\begin{aligned} \frac{\partial C_{NN}}{\partial A} &= \frac{\partial C_{NN}}{\partial C} = -\frac{C_{NN}}{A+C} \equiv K^c \\ \frac{\partial C_{NN}}{\partial B} &= -\frac{\partial C_{NN}}{\partial D} = \frac{1}{P_B}\,\frac{1}{A+C} \\ \frac{\partial C_{NN}}{\partial P_B} &= -\frac{C_{NN}}{P_B} \end{aligned}\right\} \qquad \text{(C-2)}$$

$$\frac{\partial A}{\partial F_C} = -\frac{E}{F_C} \qquad \frac{\partial B}{\partial F_C} = 0$$

$$\frac{\partial A}{\partial F_D} = +\frac{E}{F_D} \qquad \frac{\partial B}{\partial F_D} = 0$$

$$\frac{\partial A}{\partial J} = -\frac{E}{J} \qquad \frac{\partial B}{\partial J} = 0$$

$$\frac{\partial A}{\partial I_i} = \frac{1}{M} - \bar{\tau}\frac{\partial B}{\partial I_i} = \frac{1}{\gamma M}\left(\gamma - \bar{\tau} Q_i\right)$$

$$\frac{\partial B}{\partial I_i} = \frac{Q_i}{\gamma M}$$

$$\frac{\partial A}{\partial \tau_i} = -B\frac{m_i}{M} - \bar{\tau}\frac{\partial B}{\partial \tau_i} = \frac{1}{\gamma M} G$$

$$\frac{\partial B}{\partial \tau_i} = \frac{1}{\gamma M} H$$

where we have used the following definitions

$$M \equiv \sum m_i$$

$$\gamma \equiv \overline{\tau^2} - \bar{\tau}^2$$

$$Q_i \equiv \tau_i - \bar{\tau}$$

$$E \equiv \bar{F}_c \frac{J}{F_D}$$

$$G \equiv -B\gamma m_i - \bar{\tau} H$$

$$H \equiv I_i - m_i\left(\bar{I} + 2 Q_i B\right).$$

The error in class 1 is the statistical error in I_i, given by

$$\Delta I_i = \sqrt{I_i}$$

We find

$$\left(\Delta C_{NN}\right)^2 = \sum_i \left(\frac{\partial C_{NN}}{\partial A}\frac{\partial A}{\partial I_i} + \frac{\partial C_{NN}}{\partial B}\frac{\partial B}{\partial I_i} + \cdots \right)^2 \left(\Delta I_i\right)^2$$

$$= \left(K^c\right)^2 \left[\left(\sum_i R_i^c\right)^+ + \left(\sum_i R_i^c\right)^- \right] \quad \text{(C-3)}$$

where we have defined

$$R_i^c \equiv \frac{I_i}{M^2}\left[\frac{Q_i}{\gamma}\left(\bar{\tau} \oplus \frac{1}{P_B C_{NN}}\right) - 1\right]^2$$

and the superscripts (±) on the parentheses indicate the beam polarization for the quantities within. The symbol $\oplus$ signifies that the sign is to be that of the beam polarization.

The errors in class 2 are due to two sources, the random error in the target polarization for each run $\Delta\tau_i$ and the error due to F_C. These are

$$\left(\Delta C_{NN}\right)^2 = \left(k^c\right)^2 \left[\left(\sum_i S_i^c\right)^+ + \left(\sum_i S_i^c\right) \right] \left(\frac{\Delta\tau}{\tau}\right)_2^2 \quad \text{(C-4)}$$

due to τ_i, where S_i^c is defined by

$$S_i^c \equiv \left(\frac{Q_i}{\gamma M}\right)^2\left[H\left(\bar{\tau}\oplus\frac{1}{P_B C_{NN}}\right)+B\gamma m_i\right]^2$$

and we have used

$$\Delta\tau_i = \left(\frac{\Delta\tau}{\tau}\right)_2 Q_i$$

since $\bar{\tau}$ is small. Clearly the factor B is replaced by D for the the terms S_i^c of negative beam polarization. The error due to F_C is

$$\left(\Delta C_{NN}\right)^2 = \left(K^c\right)^2\left[\left(\frac{E^2}{F_c}\right)^+ + \left(\frac{E^2}{F_c}\right)^-\right] \qquad \text{(C-5)}$$

The error in class 3 is due to J and is given by the expression

$$\left(\Delta C_{NN}\right)^2 = \left(K^c\right)^2\left[\left(\frac{E^2}{J}\right)^+ + \left(\frac{E^2}{J}\right)^-\right] \qquad \text{(C-6)}$$

In class 4 there are three distinct sources of error, namely F_D, the systematic error in τ_i, and the error in P_B. The F_D error is given by

$$\left(\Delta C_{NN}\right)^2 = \left(K^c\right)^2\left[\left(\frac{E^2}{F_D}\right)^+ + \left(\frac{E^2}{F_D}\right)^-\right], \qquad \text{(C-7)}$$

that due to systematic error in τ_i by

$$\left(\Delta C_{NN}\right)^2 = C_{NN}^{\ 2}\left(\frac{\Delta\tau}{\tau}\right)_4^2 \qquad \text{(C-8)}$$

and similarly

$$\left(\Delta C_{NN}\right)^2 = C_{NN}^{\ 2}\left(\frac{\Delta P_B}{P_B}\right)^2 \qquad \text{(C-9)}$$

If we redefine the quantities K^c, S_i^c, and R_i^c, Eqs. (C-3) through (C-8) apply directly to the other computed parameters, namely $P(\theta)$, P_B, and $C_{NN}(\theta)$(internal P_B), collectively called X. We therefore have, most generally, for

class 1:

$$(\Delta X)^2 = (K^X)^2\left[\left(\sum R_i^X\right)^+ + \left(\sum R_i^X\right)^-\right],$$

class 2:

$$(\Delta X)^2 = (K^X)^2\left[\left(\sum S_i^X\right)^+ + \left(\sum S_i^X\right)^-\right]\left(\frac{\Delta\tau}{\tau}\right)_2^2,$$

as well as

$$(\Delta X)^2 = (K^X)^2\left[\left(\frac{E^2}{F_C}\right)^+ + \left(\frac{E^2}{F_C}\right)^-\right],$$

class 3:

$$(\Delta X)^2 = (K^X)^2\left[\left(\frac{E^2}{J}\right)^+ + \left(\frac{E^2}{J}\right)^-\right],$$

class 4:

$$(\Delta X)^2 = (K^X)^2\left[\left(\frac{E^2}{F_D}\right)^+ + \left(\frac{E^2}{F_D}\right)^-\right],$$

as well as

$$(\Delta X)^2 = X^2\left(\frac{\Delta\tau}{\tau}\right)_4^2.$$

Here we need to define the following quantities:

For X = P(θ):

$$K^P \equiv \frac{P}{A+C}$$

$$R_i^P \equiv \frac{I_i}{M^2}\left[\frac{Q_i}{\gamma}\left(\bar{\tau}+\frac{1}{P}\right)-1\right]^2$$

$$S_i^P \equiv \left(\frac{Q_i}{\gamma M}\right)^2\left[H\left(\bar{\tau}+\frac{1}{P}\right)+B\gamma m_i\right]^2.$$

For X = P_B:

$$K^B \equiv \frac{1}{B+D}$$

$$R_i^B \equiv \frac{I_i}{M^2}\left[\frac{Q_i}{\gamma}\left(\bar{\tau}\oplus P_B\right)-1\right]^2$$

$$S_i^B \equiv \left(\frac{Q_i}{\gamma M}\right)^2\left[H\left(\bar{\tau}\oplus P_B\right)+B\gamma m_i\right]^2.$$

For X = $C_{NN}(\theta)$ (internal P_B):

$$K^C \equiv \frac{C_{NN}}{A+C}$$

$$R_i^C \equiv \frac{I_i}{M^2}\left[\frac{Q_i}{\gamma}\left(A\bar{\tau}+\frac{B}{C_{NN}}\right)-A\right]^2$$

$$S_i^C \equiv \left(\frac{Q_i}{\gamma M}\right)^2\left[H\left(A\bar{\tau}+\frac{B}{C_{NN}}\right)+AB\gamma m_i\right]^2.$$

REFERENCES

1. Michael J. Moravcsik, The Two-Nucleon Interaction (Clarendon Press, Oxford, 1963) (Oxford Library of the Physical Sciences).
M. H. MacGregor, M. J. Moravcsik, and H. P. Stapp, Nucleon-Nucleon Scattering Experiments and their Phenomenological Analysis, Ann. Rev. Nuclear Sci. 10, 291 (1960).
Michael J. Moravcsik and H. Pierre Noyes, Theories of Nucleon-Nucleon Elastic Scattering, Ann. Rev. Nuclear Sci. 11, 95 (1961).

2. L. Wolfenstein, Polarization of Fast Nucleons, Ann. Rev. Nuclear Sci. 6, 43 (1956).

3. Henry Pierre Stapp, The Theory and Interpretation of Polarization Phenomena in Nuclear Scattering (Ph. D. thesis) UCRL-3098, Aug. 1955.
Henry P. Stapp, Relativistic Theory of Polarization Phenomena, Phys. Rev. 103, 425 (1956).

4. Clifford R. Schumacher and Hans A. Bethe, Usefulness of Polarized Targets and the Polarization Transfer Tensor in Reconstruction of the Nucleon-Nucleon Scattering Matrix, Phys. Rev. 121, No. 5, 1534 (1961).

5a. A. Abragam, M. Borghini, P. Catillon, J. Coustham, R. Roubeau et J. Thiron, Diffusion de Protons Polarises de 20 MeV par une Cible de Protons Polarises et Mesure Preliminaire du Parametre C_{nn}, Phys. Letters 2, No. 7, 310 (1962).

5b. I. M. Vasilevskii, V. V. Vishnyakov, E. Ilescu, and A. A. Tyapkin, Coefficient of Spin Correlation in pp scattering at 310 MeV and 90° in the C. M. S., Soviet Physics-JETP (U.S.A.) 12, 616 (1961).

5c. J. V. Allaby, A. Ashmore, A. N. Diddens and J. Eades, A Measurement of the Spin Correlation Coefficient C_{nn} in p-p Scattering at 320 MeV, for 90° Centre of Mass Scattering Angle, Proc. Phys. Soc. (G.B) 74, pt. 4, 482 (1959).

5d. A. Ashmore, A. N. Diddens, G. B. Huxtable and K. Skarsvag, A Measurement of the Spin Correlation Coefficient C_{nn} in p-p Scattering at 382 MeV, for 90° Centre of Mass Scattering Angle, Proc. Phys. Soc. (G.B.) 72, pt. 2, (1958).

5e. E. Engels, Jr., T. Bowen, J. W. Cronin, and R. L. McIlwain and Lee G. Pondrom, Measurement of Spin Correlation in Proton-Proton Scattering at 400 and 450 MeV, Phys. Rev. 129, No. 4, 1858 (1963).

5f. Golovin, B. M., Dzhelepov, V. P., Zul'karneev, R. Ya, Wa-Ch'uang, Ts'ui, Angular Dependence of the Polarization C_{nn} and Construction of the Amplitude Moduli for pp Scattering at 640 MeV. Estimate of the Singlet Phase Shifts II, Soviet Physics-JETP (U.S.A.) 17, 98 (1963).

6. E. F. Beall, B. Cork, P. G. Murphy, and W. A. Wenzel and C. M. P. Johnson and L. J. Koester, Jr., Polarization in π-p Scattering between 500 and 940 MeV, Phys. Rev. 126, No. 4, 1554 (1962). Richard D. Eandi, Thomas J. Devlin, Robert W. Kenny, Paul G. McManigal, Burton J. Moyer, Polarization of Recoil Protons in $\pi^{\pm}$p Elastic Scattering near 600 MeV, Phys. Rev. 136B , No. 2, 536 (1964).

7. Claude H. Schultz, Scattering of 250-MeV Positive Pi Mesons from a Polarized Proton Target (Ph. D. thesis), UCRL-11149, Jan. 1964.

8. Carson D. Jeffries, Dynamic Nuclear Orientation (Interscience Publishers, Inc., New York, 1963).

9a. Herbert M. Steiner, Frederick W. Betz, Owen Chamberlain, Byron D. Dieterle, Paul D. Grannis, Claude H. Schultz, Gilbert Shapiro, Ludwig Van Rossum, David M. Weldon, Polarization in Proton-Proton Scattering Using a Polarized Target, Part II, in Proceedings of the 1964 International Conference on High Energy Physics, Dubna, U.S.S.R., Aug. 1964 (to be published).

9b. Fred W. Betz, Polarization Parameter in Proton-Proton Scattering from 328 to 736 MeV (Ph. D. thesis) UCRL-11565, Aug. 1964. A brief summary of these two experiments is also available as UCRL-11440, June 1964.

10. S. Mandelstam, A Resonance Model for Pion Production in Nucleon-Nucleon Collisions at Fairly Low Energies, Proc. Roy. Soc. (G.B.), Series A, 244, No. 1239, 491 (1958).

11. Beers, Yardley, Introduction to the Theory of Error (Addison-Wesley Pub. Co., Cambridge, Mass., 1953).

12. M. G. Mescheryakov, S. B. Nurushev, G. D. Stoletov, Soviet Physics--JETP 6, 37 (1958).

13. Yogiro Hama and Norio Hoshizaki, p-p Scattering at 660 MeV - Modified Analysis, Research Institute for Fundamental Physics, Kyoto University, Kyoto, Japan, RIFP-30, Dec. 1963.

14. H. P. Stapp, T. J. Ypsilantis, and N. Metropolis, Phase-Shift Analysis of 310-MeV Proton-Proton Scattering Experiments, Phys. Rev. 105, No. 1, 302 (1957).

15. G. Breit, M. H. Hull, K. E. Lassila, K. D. Pyatt, Jr., Phase-Parameter Representation of Proton-Proton Scattering from 9.7 to 345 MeV, Phys. Rev. 120, No. 6, 2227 (1960).

16. H. P. Stapp, H. P. Noyes, M. J. Moravcsik, Energy Dependent Modified Phase Shift Analysis of Low Energy Proton-Proton Scattering, p. 131-4 of 1962 International Conference on High Energy Physics at CERN. Geneva, European Organization for Nuclear Research, 1962.